PLOS Biology

RESEARCH ARTICLE

Non-peptide dysbiosis metabolites reprogram a peptide quorum-sensing receptor to induce sustained predation in beneficial streptococci

Guillaume Cerckel[1], Denis Dereinne[1], Laura Ledesma-García[1], Vincent Meuric[2], Benoît Desguin[1], Johann Mignolet[1,3], Patrice Soumillion[1], Pascal Hols[1]*

1 Louvain Institute of Biomolecular Science and Technology, Biochemistry and Genetics of Microorganisms, Université catholique de Louvain, Louvain-La-Neuve, Belgium, **2** Nutrition Metabolisms and Cancer, INSERM, INRAE, Université de Rennes 1, CHU. de Rennes, Rennes, France, **3** Department of Fundamental Microbiology, Faculty of Biology and Medicine, University of Lausanne, Lausanne, Switzerland

* Pascal.Hols@uclouvain.be

OPEN ACCESS

Citation: Cerckel G, Dereinne D, Ledesma-García L, Meuric V, Desguin B, Mignolet J, et al. (2026) Non-peptide dysbiosis metabolites reprogram a peptide quorum-sensing receptor to induce sustained predation in beneficial streptococci. PLoS Biol 24(3): e3003718. https://doi.org/10.1371/journal.pbio.3003718

Academic Editor: Matthew Brent Neiditch, Rutgers Biomedical and Health Sciences, UNITED STATES OF AMERICA

Received: November 24, 2025

Accepted: March 4, 2026

Published: March 13, 2026

Data availability statement: All data are contained within the manuscript and its Supporting information files. All numerical data and statistical analyses are provided as S1 Data. All

Abstract

Cytoplasmic receptors of the RRNPPA superfamily mediate peptide-based quorum sensing in Gram-positive bacteria and are thought to be activated exclusively by short, unmodified pheromones. Here, we show that the RRNPPA regulator ComR in the human commensal *Streptococcus salivarius* can also be activated by a distinct class of non-peptide metabolites. A screen of ~200 organic compounds identified hydroxyphenylacetic acid (HPAA)—a microbial dysbiosis-associated catabolite—as a potent activator of ComR. Using biochemical and genetic approaches, we demonstrate that HPAA and related aromatic carboxylic acids bind the canonical pheromone pocket and induce sustained expression of predatory bacteriocins, while bypassing the competence program triggered by the native peptide signal (XIP). We further show that the oral pathogen *Porphyromonas gingivalis* produces physiologically relevant amounts of (H)PAA, enabling metabolite-driven activation of predation in *S. salivarius*. These findings reveal an unexpected capacity of RRNPPA receptors to sense both peptide and metabolite cues, uncovering a chemical mode of interspecies communication that links dysbiosis to predatory behavior in the oral microbiome.

Introduction

In the complex and competitive environment of the human oral cavity, *Streptococcus salivarius* is a key commensal that is recognized for its beneficial role(s) in the homeostasis of this peculiar ecological niche [1–4]. The oral cavity is a highly dynamic habitat, occupied by more than 700 bacterial species, which demands adaptive strategies for survival and colonization [3]. *S. salivarius* has developed sophisticated mechanisms to thrive and compete effectively in this challenging environment [1,3]. For instance, its ability to initiate natural transformation, to form biofilm, and its

original images used in figures are provided as S1 Raw Images.

Funding: This study was funded by the PDR grants T.0110.18/T.0111.22 and CDR grant J.0090.21 (awarded to PH) from the Belgian National Fund for Scientific Research (FNRS, https://www.frs-fnrs.be/en/). This work was also supported by the Concerted Research Actions (ARC) grants 17/22-084 and 22/27-120 (awarded to PH) from Federation Wallonia-Brussels (FWB, http://www.recherchescientifique.be/). GC held a doctoral fellowship from FNRS (FRIA fellowship). JM received funding from the European Union's Horizon 2020 research and innovation program (https://research-and-innovation.ec.europa.eu, Marie Skłodowska-Curie grant N° 101018461). The funders had no role in study design, data collection and analysis, or preparation of the manuscript.

Competing interests: I have read the journal's policy and the authors of this manuscript have the following competing interests. LLG, JM, and PH declare that they are listed as inventors on patent(s) or patent application(s) related to bacteriocin production and uses. PH and BD are, respectively, Research Director and Research Associate at the FNRS.

Abbreviations: CDM, chemically-defined medium; CSP, competence signaling peptide; DMSO, dimethyl sulfoxide; EMSA, Electrophoretic Mobility Shift Assays; HPAA, hydroxyphenylacetic acid; HTH, helix-turn-helix; QS, quorum sensing; TPR, tetratricopeptide repeats.

predation behavior through bacteriocin production are of prime importance [2,5–8]. Most of those key processes are regulated by quorum sensing (QS) to synchronize a response at the population level [7–10]. However, competence and predation have adverse effects in the short term on cellular metabolism, implying that they are tightly regulated in time and space by local environmental stimuli and stress conditions [8–12].

Two signaling systems regulate competence in streptococci, ComCDE and ComRS [9,13]. Both regulatory pathways rely on the cytosolic production and extracellular export of a genome-encoded small signaling peptide [9]. This pheromone is only active after secretion and maturation. The ComCDE system is found in mitis and anginosus groups of streptococci [9,13] and activated by the competence signaling peptide (CSP) through a phosphorylation cascade between ComD and ComE. The phosphorylated form of the transcriptional regulator ComE will then induce transcription of *comX* (master regulator of competence; alternative sigma factor σ^X) and late competence genes and, in turn, natural transformation [9,14,15]. Conversely, the ComRS system found in mutans, bovis, pyogenes, suis, and salivarius streptococcal groups [9,13] is a direct induction system [16,17] (Fig 1A). The pheromone precursor ComS is generally exported through the PptAB ABC transporter and matured by the Eep protease before its external release as a pheromone, named *sigX*/*comX*-inducing-peptide (XIP) [11,18] (Fig 1A). When it reaches a critical concentration level, XIP will in turn be internalized by the generic oligopeptide transporter Ami/Opp [19]. Then, it will bind to the cytoplasmic sensor ComR to form an active ComR·XIP complex [17]. This complex will induce *comS* to activate a positive feedback loop for the propagation of the signal and *comX* [10,19] (Fig 1A). The production of ComX will initiate the late competence phase by recruiting the RNA polymerase to activate the set of genes encoding the transformasome [9] (Fig 1A).

In addition, predation is co-activated with competence by either ComCDE or ComRS (directly or indirectly) through the production of bacteriocins and lytic enzymes in most streptococci [13]. In *S. salivarius*, those two processes are directly coregulated by the ComRS system [8]. Besides *comS* and *comX*, the ComR·XIP complex directly activates the expression of *comA* that codes for a bacteriocin transporter (operon *comS-comA*) and a range of *blp*/*slv* genes encoding a cocktail of class II bacteriocins (salivaricins) with a variable spectrum of antimicrobial activity [8] (Fig 1A). Interestingly, expression of bacteriocin genes is more responsive to lower XIP pheromone concentrations than the *comX* gene, suggesting that their production could precede competence activation to induce lysis of neighbor cells and supply exogenous DNA for natural transformation [8]. While coupling competence and predation can have advantages, streptococci are also able to uncouple the activation of predation [13,20]. In most streptococci, activation of predation alone is dependent on the QS BlpCRH system, whose activation through phosphotransfer is very similar to the ComCDE system [13,20]. In *S. salivarius*, this system is replaced by a duo of ComR-like regulators, named ScuR and SarF [7]. We have shown that the three regulators—*i.e.*, ComR, ScuR, and SarF—recognized a similar DNA palindromic motif but with a different selectivity depending on a slight sequence variation of the binding

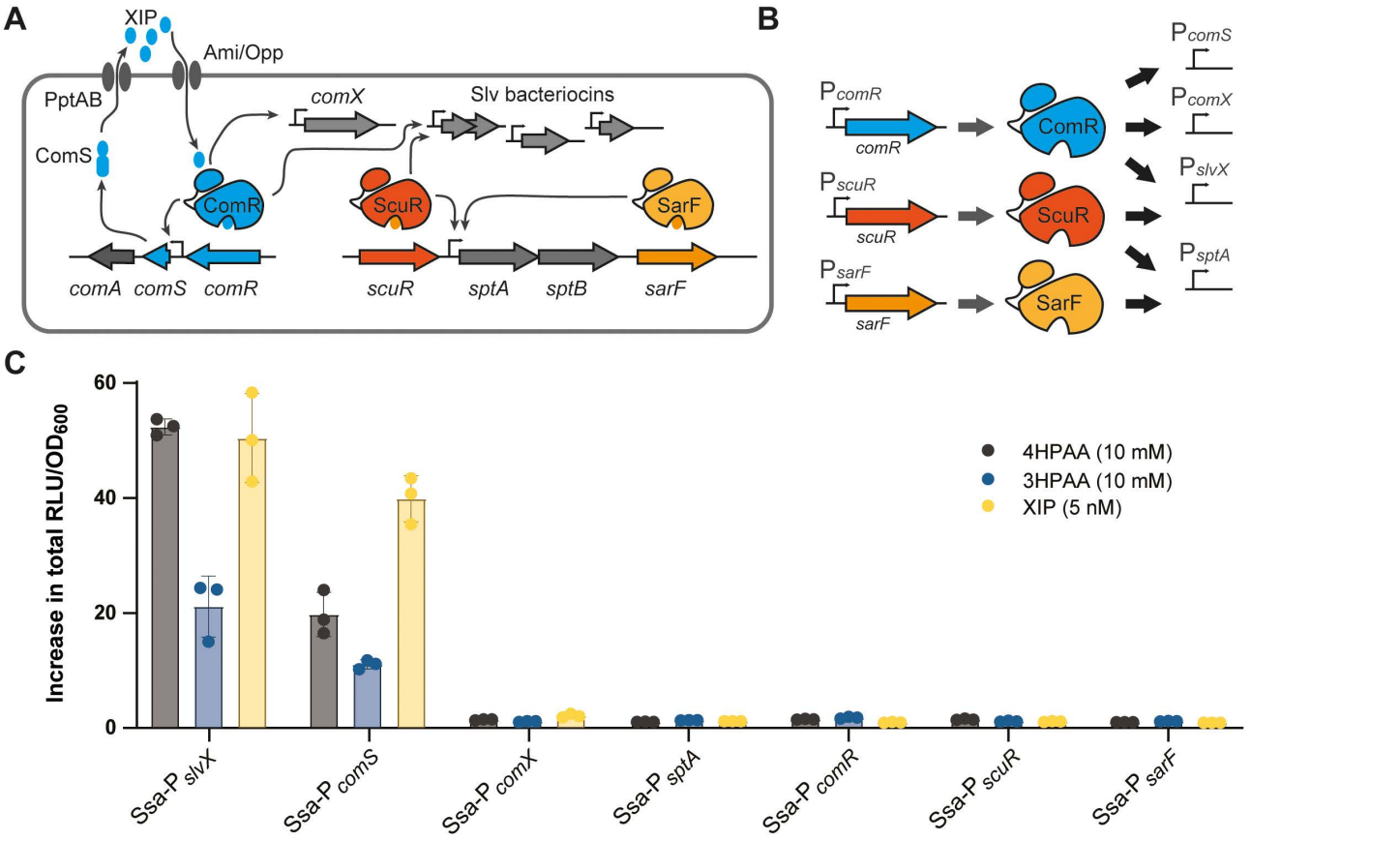

Fig 1. 4HPAA and 3HPAA are inducers of predation in *S. salivarius*. A. Scheme illustrating activation of early competence and predation in *S. salivarius* (Ssa). A basal level of *comS* expression will lead to XIP pheromone accumulation in the medium. When XIP reaches a critical concentration, its reimportation will lead to ComR activation. In turn, it will induce *comS* to amplify XIP production (positive feedback loop) and *comX*, resulting in DNA transformation. It will also coactivate a suite of bacteriocin promoters (*e.g.*, P_{slvX}) linked to predation. In parallel, activated ScuR is also able to induce bacteriocin genes. In addition, *sptAB,* encoding a bacitracin-like ABC transporter, is induced by both ScuR and SarF. **B.** For the screen, we used the promoters of *comR*, *scuR*, and *sarF* genes. We also used P_{comX} (only bound by ComR), P_{slvX} (bound by ComR and ScuR), and P_{sptA} (bound by ScuR and SarF). P_{comS} was not used for the screen but only for validation of *comA* expression (bacteriocin exporter gene). **C.** Luminescence assays of P_{slvX}, P_{comS}, P_{comX}, P_{sptA}, P_{comR}, P_{scuR}, and P_{sarF} reporter fusions (*luxAB*) in response to 4-hydroxyphenylacetic acid (4HPAA; 10 mM), 3-hydroxyphenylacetic acid (3HPAA, 10 mM), and XIP (5 nM). Reporter strains were grown in CDMG. The fold increase in total luminescence (RLU/OD_{600}) was calculated between induced and non-induced conditions. Data are mean values of biological triplicates (dots) ± standard deviation (error bars). The data underlying this Figure can be found in S1 Data.

https://doi.org/10.1371/journal.pbio.3003718.g001

site (*i.e.*, ComR box) and its relative position in the promoter sequence [7]. For instance, ScuR can activate the bacteriocin genes without activating the *comX* gene, allowing the uncoupling of predation activation from competence triggering [7] (Fig 1A). While ComR is activated by the XIP pheromone, the native peptide(s) activating ScuR and SarF remain(s) unknown [7]. However, we were able to select a range of synthetic activating peptides (sBI7 peptide as prototype) from a mutant library able to selectively activate ScuR/SarF without activating ComR [7]. ComR and these two ComR-like regulators are members of a distinct family among RRNPPA (Rap, Rgg, NprR, PlcR, PgrX, AimR) cytoplasmic sensors, whose mode of activation has been deeply investigated at the biochemical level [21–24]. ComR family members are composed of two domains, the DNA-binding domain (HTH, helix-turn-helix) connected by a linker to the peptide-binding domain (TPR, tetratricopeptide repeats) [17]. The TPR domain binds the peptide inside a hydrophobic pocket, whose residues

involved in specific interactions with the inducing peptide have been deeply investigated at the structural level [16,17,25]. The peptide binding induces a range of conformational changes that eventually allow HTH release from TPR interaction, TPR dimerization, and DNA binding [17].

The ComRS and ScuR/SarF systems of *S. salivarius* can only be activated under laboratory conditions by adding their inducing peptides [7,8]. Recently, we showed that the ComRS system of *S. salivarius* is under the strict control of the general stress-sensing system CovRS, indicating that perceiving the right combination of external stimuli from the environment is a key aspect for competence/predation activation [10]. Knowing the importance of nutrient availability on the physiology of *S. salivarius* [4,26,27], we here explored the impact of a range of carbon/nitrogen sources on the modulation of ComRS and ScuR/SarF systems. From around 200 growth conditions, we unexpectedly identify hydroxyphenylacetic acids as direct inducers of the ComR regulator. With mobility shift assays, modeling, and in vivo tests, we dissected the chemical moiety responsible for activation and extended the inducers to a family of carboxylic acids derived from hydrophobic amino acids. Those molecules, naturally produced in cases of dysbiosis by anaerobic proteolytic bacteria from the digestive tract [28–30], trigger an unconventional sustained predation response in salivarius streptococci without activating DNA transformation. This dual activation of ComR (cognate pheromone for QS and small organic molecules for dysbiosis sensing) highlights the flexibility of cytoplasmic sensors to respond to multiple stimuli for the maintenance of the microbial homeostasis in the digestive tract.

Results

Hydroxyphenylacetic acids trigger predation in *S. salivarius*

ComR(-like) and structurally-related Rgg sensors are predominant members of the RRNPPA superfamily in streptococci [21,22,31], which are highly influenced by external signals and cell physiology. These parameters could either control the expression of the ComR/Rgg-encoding genes [10,32] or affect the formation of the active ComR/Rgg-peptide complexes, such as through the modulation of inducing peptide availability or the production of interfering peptides (Fig 1A) [11,33–35]. To explore the regulation and activation of the three paralogous sensors, ComR, ScuR, and SarF, from *S. salivarius* (Ssa) HSISS4, we designed a screening approach based on six luminescent reporter fusions inserted in an ectopic locus (Fig 1B). While a first set of fusions aims to monitor the activation of the promoters of each regulator gene (P_{comR}, P_{scuR}, and P_{sarF}, fused to *luxAB* genes), a second set reports the impact of these regulators on the activation of the downstream genes (Fig 1A and 1B). The chosen promoters were (i) P_{comX} as a proxy of competence that is specifically induced by ComR, (ii) P_{slvX} as a proxy of predation that is induced by both ComR and ScuR, and (iii) P_{sptA} controlling a bacitracin-like ABC transporter that is activated by ScuR and SarF [7] (Fig 1B). Altogether, these six fusions will allow us to monitor any direct or indirect effect of a physiological stimulus that would activate one or more of these three regulatory systems in *S. salivarius*.

Since carbon/nitrogen sources were previously shown to impact the activity of Rgg systems in various streptococci [32,36], we screened 192 molecules (*e.g.*, simple/complex sugars, amino acids and derivatives, and organic acids) using phenotype microarrays (Biolog plates PM1 and PM2A) with the six luminescent reporter strains (S1 Table and S1 Fig). As preliminary tests showed limited growth of *S. salivarius* across a wide range of carbon sources, chemically-defined medium (CDM) was supplemented with 0.15% glucose. This concentration of glucose allows an initial growth (OD_{600}~0.75), which could be increased if the tested carbon source is sequentially consumed (diauxic growth) or co-metabolized. While no major increase in luminescence was noted for P_{comR}, P_{scuR}, P_{sarF}, P_{comX}, and P_{sptA} reporter strains compared to the control (C^-, CDM with 0.15% glucose alone), two carbon sources induced luminescence with the P_{slvX} reporter strain (S1 Fig). Interestingly, 4-hydroxyphenylacetic acid (4HPAA) and 3-hydroxyphenylacetic acid (3HPAA) triggered a ~50- and ~20-fold upregulation of P_{slvX}, respectively (Fig 1C). In addition, P_{slvX} activation is not due to a higher expression of any of the three regulator genes and does not imply a coactivation of competence, as shown by the absence of P_{comX} induction (Fig 1C). Because predation by *S. salivarius* through bacteriocin production requires

co-induction of the bacteriocin exporter ComA, encoded within the *comS–comA* operon (Fig 1A), we next monitored activation of this locus. P_{comS} was also induced by the two compounds, indicating coordinated activation of the bacteriocin exporter together with its cognate bacteriocins (using P_{slvX} as a proxy) (Fig 1C).

Together, these results show that predation via the activation of genes encoding bacteriocins and their exporter is stimulated by two small organic acids, 4HPAA and 3HPAA, which are not produced by *S. salivarius* but are known as byproducts or intermediates in the catabolism of aromatic amino acids of many anaerobic bacteria ([37] and KEGG database).

4HPAA induces predation through ComR

Since the presence of 4HPAA has been reported as a biomarker of microbial dysbiosis in the digestive tract due to the proliferation of proteolytic bacteria [30], this prompted us to further investigate how 4HPAA stimulates the activation of bacteriocin genes. To confirm the activation of P_{slvX}, the dynamics of its induction by 4HPAA during growth was compared to the XIP pheromone (Fig 2A). Whereas XIP addition triggered a sharp and transient activation peak during early exponential growth, as previously reported [8], 4HPAA induced a more sustained activation throughout exponential growth, consistent with a distinct mode of signal perception. We therefore examined whether these two modes of activation could interact in an additive, synergistic, or competitive manner. When a low concentration of XIP (5 nM) was combined with 4HPAA (1 mM), bacteriocin gene expression displayed a prolonged activation profile, reflecting the combined contributions of both signals (S2A Fig). Interestingly, under these conditions, 4HPAA partially antagonized XIP signaling, leading to an approximately 2-fold reduction of the XIP-induced response, without markedly affecting the overall level of bacteriocin expression (S2B Fig). At higher XIP concentrations (25 nM), this antagonistic effect of 4HPAA was no longer observed (S2C Fig). However, increasing the concentration of 4HPAA (7.5 mM) restored the inhibitory effect (S2D Fig), indicating a strong and dose-dependent interplay between the two inducers. Given that P_{slvX} could be activated by either ComR or ScuR, we examined the impact of 4HPAA on various deletion mutants (Fig 2B). The deletion of *comR* (Δ*comR*) led to a complete absence of P_{slvX} induction by 4HPAA. In contrast, the deletion of *comS* (Δ*comS*) did not alter the 4HPAA response, indicating that neither the XIP precursor nor the mature XIP is required for this regulatory pathway. In addition, the deletion of *scuR* and *sarF* genes (Δ*scuR-sarF*) had no impact on 4HPAA stimulation. Altogether, these results show that 4HPAA specifically activates the cytoplasmic sensor ComR.

Bacteriocin assays were also performed to confirm that 4HPAA effectively induces a genuine predation response. We tested the wild-type strain, a mutant strain with all five bacteriocin loci deleted (Δ*slv5*; negative control), a mutant constitutively expressing bacteriocins (P_{32}-*scuR*; positive control), the Δ*comR* mutant, and the double Δ*scuR-sarF* mutant. Four experimental conditions were evaluated: no inducer, addition of XIP (1 μM), sBI7 (1 μM), or 4HPAA (10 mM) (Fig 2C). With XIP addition, a ComR-specific inducing peptide, both the wild type and the Δ*scuR-sarF* mutant produced inhibition halos, but not the Δ*comR* mutant. Conversely, with the addition of the sBI7 peptide, which is ScuR/SarF-specific, the wild type and the Δ*comR* mutant exhibited inhibition halos, but not the Δ*scuR-sarF* mutant. Notably, the addition of 4HPAA phenocopies the XIP effect, confirming that the 4HPAA response is strictly ComR-dependent. We also evaluated bacteriocin production in response to an increasing concentration of 4HPAA (Fig 2D). In the wild type, an inhibition halo was detected at a concentration of 0.5 mM, and its size gradually increased up to 10 mM. Given that ComR activation by XIP leads to a coupling between predation and competence [8], we also evaluated the capacity of 4HPAA to induce natural DNA transformation in *S. salivarius*. 4HPAA-induced cells (10 mM) failed to generate any detectable transformant in standard conditions (S2E Fig), corroborating the absence of P_{comX} activation by 4HPAA (Figs 1C and S2F).

Altogether, these results show that 4HPAA is exclusively perceived by ComR through a pathway that is independent of the XIP pheromone. Moreover, the selective activation of predation via ComR without competence induction is an exclusive feature of the 4HPAA-inducing response.

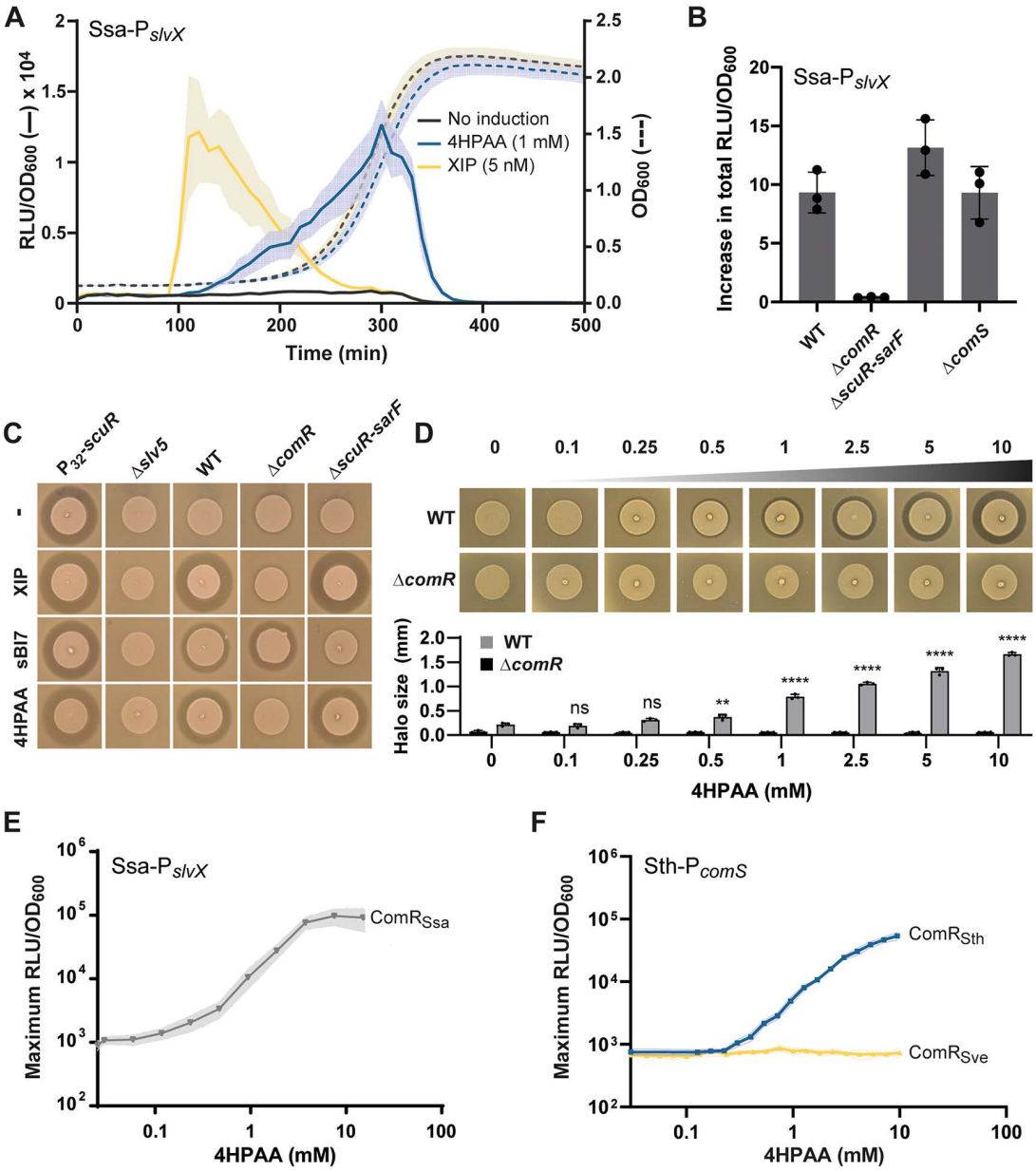

Fig 2. 4HPAA activates predation through ComR in salivarius streptococci. A. Luminescence (RLU/OD_{600}) over time of the *S. salivarius* (Ssa) P_{slvX}-*luxAB* reporter fusion without inducer, with 4HPAA (1 mM), or with XIP (5 nM). **B.** Fold increase in total luminescence between 4HPAA induction (10 mM) and non-induced conditions for the *S. salivarius* P_{slvX} reporter strain (WT) and its derivative mutants (Δ*comR*, Δ*scuR-sarF*, and Δ*comS*). **C.** Bacteriocin assays with wild type (WT) and mutants P_{32}-*scuR* (positive control), Δ*slv5* (negative control), Δ*comR*, and Δ*scuR-sarF* without inducer (−), with 1 μM XIP (ComR-specific), 1 μM sBI7 (ScuR/SarF-specific), or 10 mM 4HPAA. *Lactococcus lactis* IL1403 was used as an indicator strain. **D.** Bacteriocin assays with increasing concentrations of 4HPAA (0 to 10 mM) on wild type (WT) and Δ*comR* mutant (negative control). Indicator strain as in panel **C.** The bottom graph shows the size of inhibition zones (mm). **E.** and **F.** Maximum luminescence in response to a 4HPAA gradient (0 to 10 mM) for *S. salivarius* (Ssa) P_{slvX}-*luxAB* ($ComR_{Ssa}$) (panel **E**), *S. thermophilus* (Sth) P_{comS}-*luxAB* Δ*comS* ($ComR_{Sth}$), and its isogenic strain *comR::comR*$_{Sve}$ ($ComR_{Sve}$) (panel **F**). Data presented in panels A, B, D, E, and F are mean values of biological (panels A, B, E, and F) or technical replicates (panel **D**) ± standard deviation (error bars in panel B and D, and light color zones in panels A, E, and **F**). In panel D, the inhibition zones induced by 4HPAA were statistically compared to the WT without 4HPAA using One-Way ANOVA with Dunnett's test (** $P < 0.01$; **** $P < 0.0001$; ns, non-significant). The data underlying this Figure can be found in S1 Data.

https://doi.org/10.1371/journal.pbio.3003718.g002

4HPAA induction is ComR-specific among salivarius streptococci

S. salivarius, *Streptococcus thermophilus* (Sth), and *Streptococcus vestibularis* (Sve) are closely related species forming the salivarius group [1]. This is evident from the high similarity among their respective ComR proteins. Indeed, $ComR_{Ssa}$ and $ComR_{Sth}$ display a very high level of identity (95%) and are both activated by the same XIP peptide ($XIP_{Ssa/Sth,}$ LPYFAGCL) [19]. $ComR_{Sve}$ is more distantly related (83% of identity with $ComR_{Ssa}$) and is strictly induced by a variant XIP peptide (XIP_{Sve}, VPFFMIYY) [16]. To test the HPAA response, we used three reporter strains, each encoding a different homolog of ComR: *S. salivarius* P_{slvX}-*luxAB* for $ComR_{Ssa}$ (positive control), *S. thermophilus* P_{comS}-*luxAB* (Δ*comS*) for $ComR_{Sth}$, and a variant version of the previous strain where $ComR_{Sth}$ was exchanged by $ComR_{Sve}$ ($comR_{Sth}$::$comR_{Sve}$) [16]. The two isogenic strains of *S. thermophilus* were previously validated for the strict response (P_{comS} activation) of their ComR version to XIP_{Sth} and XIP_{Sve}, respectively [16]. We tested a gradient of 4HPAA (0–10 mM) on these three reporter strains (Fig 2E and 2F). For $ComR_{Ssa}$ and $ComR_{Sth}$ reporter strains, an increase in luminescence started in the range of 100–500 μM with a maximum achieved at ~8–10 mM. Interestingly, the third reporter strain encoding $ComR_{Sve}$ did not respond to 4HPAA at any tested concentration (Fig 2F).

Since the more distant ortholog of ComR ($ComR_{Sve}$) is insensitive, these results show that the 4HPAA response is not only ComR-dependent but also ComR-specific, which points towards a direct interaction between 4HPAA (or a derivative compound) and ComR for its activation.

4HPAA activates ComR in vitro

There was no prior evidence for direct interactions between RRNPPA regulators and organic acids as inducers. Therefore, we were prompted to investigate the direct binding of 4HPAA to ComR in vitro. Since $ComR_{Sth}$ and $ComR_{Ssa}$ behave similarly in vivo, we used $ComR_{Sth}$ based on its extensive biochemical characterization [16,17,25]. We performed Electrophoretic Mobility Shift Assays (EMSA) with purified $ComR_{Sth}$ (and $ComR_{Sve}$ used as a negative control), a fluorescent $^{Cy3}P_{comS}$ DNA probe, and 4HPAA (or XIP_{Sth} used as a positive control) as inducer of complex assembly [16,17] (Figs 3A and S3). In these experiments, we added 4HPAA at a single concentration directly into the running buffer to ensure a homogenous distribution of the molecule. We used gradients of $ComR_{Sth}$ and $ComR_{Sve}$ (noting that an excess of ComR leads to its precipitation) along with a fixed amount of the DNA probe and performed migration in buffers with and without 4HPAA (10 mM). As a positive control, we also used conditions with a fixed concentration of $ComR_{Sth}$ and a gradient of XIP_{Sth} to visualize the position of the ComR·XIP complex. Notably, $ComR_{Sth}$ in the presence of 4HPAA led to the formation of a specific complex with similar mobility compared to the XIP_{Sth} positive control (Fig 3A). Conversely, $ComR_{Sve}$, which does not respond to 4HPAA in vivo (Fig 2D), displayed no high molecular size complex (S3 Fig).

Together, these results showed the direct binding of 4HPAA to ComR, resulting in the formation of an active complex able to bind DNA. To the best of our knowledge, a chemical compound has never been reported to directly activate a regulator of the RRNPPA family.

4HPAA is predicted to occupy the XIP C-terminus binding site for ComR activation

To investigate how 4HPAA could interact with ComR, we ran *in silico* docking predictions using the EADock DSS engine from SwissDock [38]. We used the anionic form of 4HPAA and compared docking predictions for the crystal structures of $ComR_{Sth}$ and $ComR_{Sve}$ holoforms (XIP-activated), and $ComR_{Sth}$ apoform. Remarkably, the top-ranked prediction (total energy of −17.7 kcal/mol) for holo-$ComR_{Sth}$ positioned the 4HPAA molecule deeply in the XIP binding pocket right at the site occupied by the pheromone C-terminal leucine (XIP-L8) (Fig 3B). By comparison, the predicted docking of 4HPAA in the same configuration within the XIP-binding pocket of holo-$ComR_{Sve}$ is less stable (total energy of −14.8 kcal/mol), and such positioning is not predicted in apo-$ComR_{Sth}$. The carboxylate group of docked 4HPAA is predicted to form a salt bridge with the side chain ammonium group of residue K100 from helix α7 and to H-bond with T90 from loop α6-α7 of $ComR_{Sth}$, as previously reported for the C-terminal carboxylate group of XIP-L8 (Fig 3B) [17]. In addition, the hydroxyl

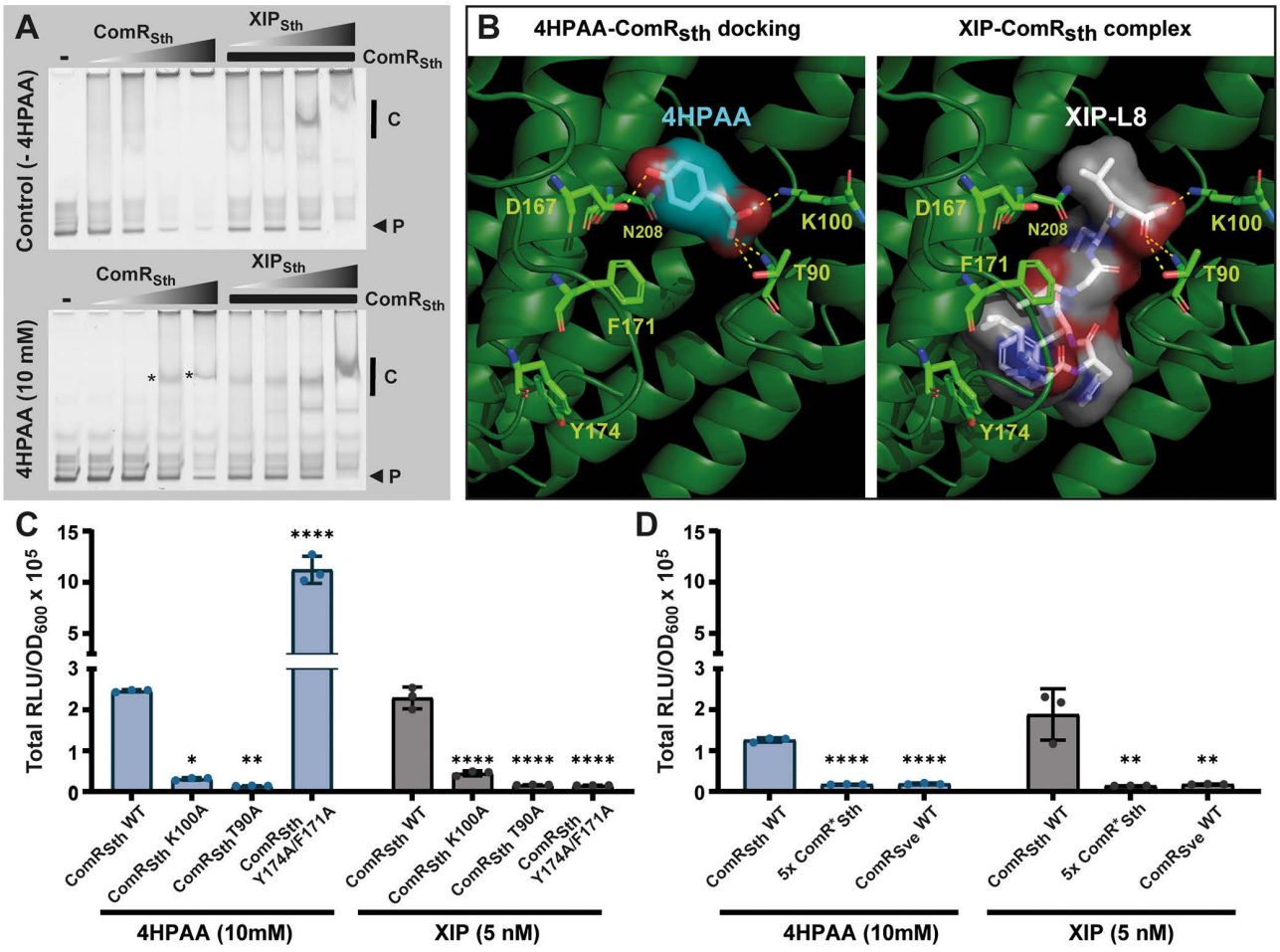

Fig 3. Direct binding of 4HPAA into the peptide pocket of ComR. A. Mobility shift assays of the *comS* promoter probe (40 ng) conducted with a gradient of purified $ComR_{Sth}$ (gray triangles, 2:2 dilutions from 4 μM) (left) or with a fixed concentration of $ComR_{Sth}$ (2 μM) and a gradient of XIP_{Sth} (gray triangles, 25, 50, 200, and 1,000 nM) (right), without (top) or with (bottom) 10 mM 4HPAA. Probes (P) indicated by a black arrow are Cy3-conjugated DNA fragments of 40 bp. Vertical back lines indicate the position of specific complexes and stars label complexes formed in the presence of 4HPAA alone. The control condition without $ComR_{Sth}$ is indicated with a minus sign (−). **B.** *In silico* prediction of 4HPAA in complex with $ComR_{Sth}$ holoform (right) compared to the native XIP-$ComR_{Sth}$ complex (PDB 5JUB) (left). The top-ranked docked 4HPAA (blue) is mimicking the positioning of XIP-L8 (white). ComR residues T90, K100, and D167 are highlighted in light green, as they were predicted to directly interact with 4HPAA (yellow dotted lines). ComR residues F171 and Y174 are shown since they are essential for the interaction with XIP. **C.** In vivo luminescence response (total RLU/OD_{600}) of $ComR_{Sth}$ wild-type (WT) and variants K100A, T90A, and Y174A/F171A to 4HPAA (10 mM) or XIP (5 nM). Experiments were performed with *S. thermophilus* P_{comS}-*luxAB* Δ*comS*. **D.** In vivo luminescence response of $ComR_{Sth}$ wild-type (WT), $ComR_{Sth}$ penta-mutant (5× $ComR^*_{Sth}$) responding only to XIP_{Sve}, and $comR_{Sve}$ WT to 4HPAA (10 mM) or XIP (5 nM). Same genetic background as in panel **C.** Dots, bars, and error bars in panels C and D show biological triplicates, mean values, and standard deviations, respectively. All variants were statistically compared to $ComR_{Sth}$ WT using one-way ANOVA with Dunnett's test (* $P < 0.05$; ** $P < 0.01$; **** $P < 0.0001$). The data underlying this Figure can be found in S1 Data.

https://doi.org/10.1371/journal.pbio.3003718.g003

group of 4HPAA is predicted to H-bond with D167 from helix α10, which could enhance its stabilization in the pocket (Fig 3B). Finally, N208 is contacting the 4HPAA aromatic ring in an adequate orientation to establish a weak H-bond with the π cloud as an acceptor (NH...πbond) [39].

We further modeled ab initio the positioning of 4HPAA in the predicted structures of various ComR proteins using the protein-ligand prediction tool Chai-1 [40] (S4 Fig). Based on the conservation of the four residues reported above (S5 Fig), we selected $ComR_{Sth}$ (used here as a positive control), $ComR_{Ssa}$, $ComR_{Sve}$, and ComR of *Streptococcus mutans*

($ComR_{Smu}$), which show perfect conservation of these residues, as well as the more distant ComR proteins from *Streptococcus pyogenes* ($ComR_{Spy}$) and *Streptococcus suis* ($ComR_{Ssu}$), which contain substitutions (*i.e.*, K100R, D167E/R, or N208K/D) (S5 Fig). While 4HPAA was predicted to adopt a similar binding mode in $ComR_{Sth}$ and $ComR_{Ssa}$, consistent with docking results obtained for holo-$ComR_{Sth}$, a distinct positioning of the ligand was observed in all other ComR homologs analyzed (S4 Fig). This difference likely reflects a suboptimal architecture of the 4HPAA-binding pocket (*e.g.*, $ComR_{Sve}$ and $ComR_{Smu}$) and/or the lack of conservation of several key interacting residues (*e.g.*, $ComR_{Spy}$ and $ComR_{Ssu}$). Altogether, these *in silico* predictions suggest that 4HPAA may preferentially bind to the XIP-binding pocket of $ComR_{Sth}$ and $ComR_{Ssa}$, whereas structural divergence in other ComR homologs likely prevents productive ligand accommodation.

We previously reported that mutating residues at the bottom (T90, K100; interaction with XIP-L8) or the top (F171/Y174; interaction with XIP-L1) of the XIP binding pocket in $ComR_{Sth}$ abolished the XIP_{Sth}-mediated activation (Fig 3B) [17,25]. Mutants T90A and K100A lost their ability to induce luminescence in response to 4HPAA, mirroring our previous observations with XIP [17] (Fig 3C). In contrast, the double Y174A/F171A mutant exhibited a 4-fold increase in light emission upon 4HPAA activation compared to the control, despite a loss of inducibility by XIP (Fig 3C). These effects are partially recapitulated in the single F171A mutant (S6 Fig). The F171A and Y174A/F171A mutants were previously shown to display a higher basal level of activation without XIP addition [25], indicating a less stringent conformational control that could explain their better activation by the remote binding of 4HPAA. In a previous work, we also generated a $ComR_{Sth}$ variant (5× ComR*) with five substitutions (R92G, V205A, S248G, S289K, and I290T) that responds exclusively to XIP_{Sve} due to a remodeling of the peptide binding pocket [16]. Our luminescence assays showed that, as observed with $ComR_{Sve}$, this $ComR_{Sth}$ variant is unable to respond to 4HPAA (Fig 3D). A dissection of individual substitutions in the XIP binding pocket showed that the R92G substitution recapitulates the loss of 4HPAA induction, as previously reported for its key role in the XIP_{Sth}-mediated activation mechanism [17] (S6 Fig). In addition, the S289K substitution showed an interesting behavior, being more reactive to 4HPAA and less sensitive to XIP_{Sth} than their respective controls (S6 Fig). The lysine at position 289 could favor initial encountering with 4HPAA to facilitate its activation effect.

Overall, this analysis supports a model where 4HPAA partially mimics the XIP activation mechanism by substituting XIP-L8 for key interactions with residues T90 and K100 in the peptide binding pocket of ComR. This alternative mode of activation is further supported by the 4HPAA ability to activate ComR mutants that are not or are weakly responding to XIP.

Carboxylic acid derivatives of bulky hydrophobic amino acids are ComR inducers

In our investigation of 4HPAA selectivity for ComR activation, we tested several structural variants of this molecule for their in vivo activation capacity with a specific focus on three key aspects: (i) the carboxylate function and its associated negative charge, (ii) the polarity around the aromatic ring, and (iii) the overall size of the molecule (Fig 4A). For variations of the carboxylate moiety, we examined tyramine (featuring a positively charged ammonium at neutral pH) and methyl-4HPAA (a neutral methylester derivative), but none of them elicited a luminescence signal (Fig 4B). This aligns with our 4HPAA-binding prediction, which suggests that the carboxylate is critical for interactions with residues T90 and K100 inside the XIP binding pocket (Fig 3B). In addition, two α-hydroxy-carboxylates, (R)-(−)-mandelic acid and D-(+)-3-phenyllactic acid, also failed to induce luminescence (Fig 4). This is in line with the structural model that predicts steric hindrance upon substituting the pro-R α-hydrogen by a bulkier group or extending the length of the carboxylate moiety. For the polarity around the aromatic ring, phenylacetic acid (PAA), which lacks a hydroxyl group, or compounds with similar steric hindrance, like 3HPAA and 3-fluoro-4HPAA (Fig 4), were able to produce luminescence, although at ~2-fold lower levels (orange bars, Fig 4B). This indicates that the presence, position, or polarity of the hydroxyl group plays a secondary role in ComR activation, suggesting that 4HPAA interaction with residue D167 is not critical. Furthermore, pentafluoro-PAA failed to induce luminescence (Fig 4B), further supporting the potential NH...π H-bond stabilization since fluorine atoms will decrease the electron density of the πcloud [39]. We also examined compounds with a larger steric hindrance than 4HPAA. The presence of

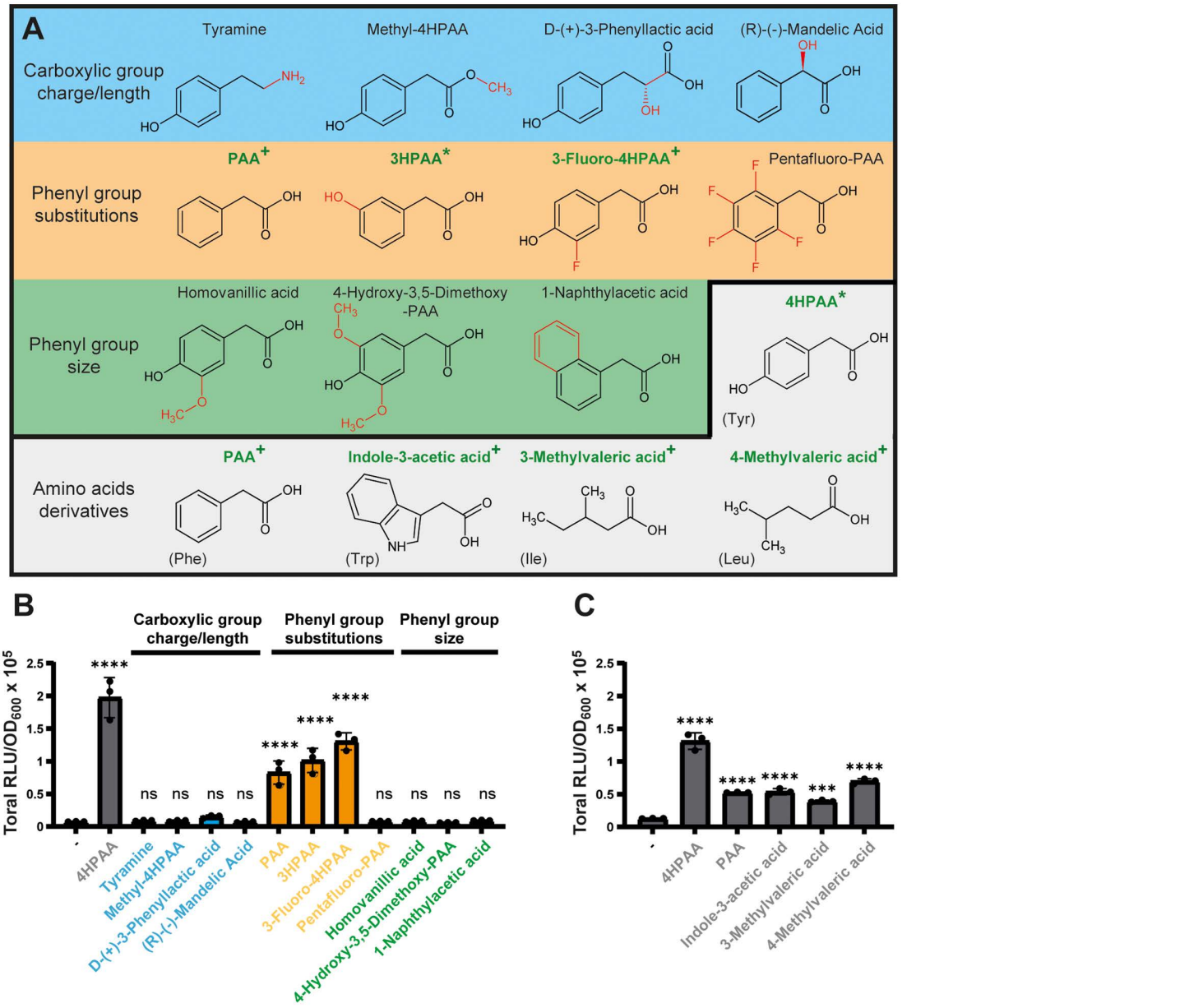

Fig 4. Extended activation of ComR by bulky derivatives of hydrophobic amino acids. A. Structure of 4HPAA variants with modifications of the carboxylic moiety (charge and length; blue rectangle), phenyl group substitutions (orange rectangle), steric hindrance (green rectangle); and hydrophobic amino acid derivatives (gray). Modified chemical groups compared to 4HPAA are highlighted in red. The names of chemicals in bold green indicate inducing molecules. The initial and new inducing molecules are labeled with * and $^{+}$, respectively **B.** Luminescence assays (total RLU/OD_{600}) with 4HPAA structural variants (10 mM) shown in panel **A**. **C.** Luminescence assays with organic acids derived from bulky hydrophobic amino acids (10 mM) shown in panel **A**. Derivatives of Tyr, Phe, Trp, Ile, and Leu induced a signal. In panels B and C, experiments were performed with *S. thermophilus* P_{comS}-*luxAB* Δ*comS*. Dots, bars, and error bars show biological triplicates, mean values, and standard deviations, respectively. All variant molecules were statistically compared to the control condition without organic acid (minus sign) using one-way ANOVA with Dunnett's test (*** $P < 0.001$; **** $P < 0.0001$; ns, non-significant). The data underlying this Figure can be found in S1 Data.

https://doi.org/10.1371/journal.pbio.3003718.g004

one or two methoxy groups in the meta position of the aromatic ring, as in homovanillic acid and 4-hydroxy-3,5-dimethoxy-PAA, or the addition of a second aromatic ring, as in 1-naphthylacetic acid, resulted in inactive compounds (Fig 4).

Since 4HPAA and PAA are two carboxylic acids derived from aromatic amino acids (Tyr and Phe), we also tested equivalent derivatives from the whole set of hydrophobic amino acids for $ComR_{Ssa/Sth}$ activation (Figs 4C and S7). In addition to 4HPAA and PAA, the bulkiest compounds, indole-3-acetic acid (IAA; Trp derivative), 3-methylvaleric acid (3MVA, Ile derivative), and 4-methylvaleric acid (4MVA, Leu derivative), were also able to increase the luminescence signal (Fig 4C), while isovaleric acid (Val derivative) with one carbon less than MVA and other amino acid derivatives of shorter length did not (S7 Fig). Among these three activating compounds, we chose 4MVA for EMSAs, which confirmed its ability to activate ComR as observed for 4HPAA (S3 Fig).

Together, these in vivo assays with 4HPAA structural variants strengthen the docking model of ComR activation, regarding (i) the key role played by the carboxylate group and hydrophobic side chain, (ii) the simulating effect of the hydroxyl group in the para position of the aromatic ring, and (iii) the size fitting of the molecule into the binding pocket. Moreover, we pinpoint five amino acid derivatives that could be of biological relevance as signaling molecules since most of them were previously identified in various human fluids associated with microbial dysbiosis [28–30,41–44].

Porphyromonas gingivalis culture supernatant triggers ComR activation

S. salivarius is a dominant commensal species of the oral cavity and the upper part of the small intestine [1,27]. In cases of microbial dysbiosis, the proliferation of gram-negative bacteria (*e.g.*, *Prevotella* sp. and *Porphyromonas* sp.) in the oral cavity or Gram-positive bacteria (*e.g.*, *Clostridium* sp.) in the small intestine was reported to incompletely catabolize aromatic amino acids, leading to increased levels of 4HPAA, PAA, or IAA in saliva, urine, or feces [30]. To evaluate if one of these bacteria could accumulate a substantial level of those compounds in their culture supernatants, we tested the well-studied opportunistic pathogen *P. gingivalis* of the oral cavity [45]. *P. gingivalis* W83 was grown under anaerobic conditions in enriched BHI medium (BHIe) until late stationary growth. Filtered supernatants were then added (25% v/v of CDM) to cultures of *S. thermophilus* and *S. salivarius* reporter strains (P_{comS}-*luxAB* and P_{slvX}-*luxAB*, respectively) for luminescence assays (Fig 5A). The *S. thermophilus* reporter strain was strongly activated by *P. gingivalis* culture supernatants (unextracted *Pg* SN, Fig 5A), while the BHIe medium alone was inefficient to stimulate light emission. In addition, culture supernatants of *P. gingivalis* grown in BHIe enriched with Phe or Tyr significantly increased the luminescence signal (~3-fold), supporting the hypothesis that byproducts of aromatic amino-acid catabolism contribute to activation (S8A Fig). We also validated that the supernatant effect was ComR-dependent and ComS/XIP-independent by using Δ*comR* and Δ*comS* mutants of the reporter strain, respectively (Fig 5B). To exclude the presence of an inducing peptide in the culture supernatant that could mimic XIP, we also used an oligopeptide transporter mutant (Δ*ami*/*opp*), which remains similarly inducible as the control strain (Fig 5B). Intriguingly, the *S. salivarius* reporter strain did not respond in the same conditions, except for a weak activation with aromatic amino acid-enriched BHIe medium (S8B Fig). We identified that the BHIe medium alone has a quenching effect on the activation of the ComRS system through a downregulation of *comR* expression (P_{comR}-*luxAB*) (S8C Fig). To counteract this effect, we used an isogenic reporter strain containing a P_{xyl2}-*comR* cassette (xylose-inducible) [10]. At a low *comR* expression level (xylose 0.2%), the *S. salivarius* reporter strain was activated by the different culture supernatants as shown above with *S. thermophilus* (S8D Fig).

Since these results converged towards the presence of aromatic amino-acid derivatives in the supernatant, we performed an ethyl acetate extraction at low pH to selectively extract hydrophobic acids such as HPAA, PAA, and IAA [46] for their analysis by capillary electrophoresis. We showed that the extracted fraction was still able to generate a specific luminescence signal (extracted *Pg* SN, Fig 5A) and appeared to contain a mixture (~1:1) of HPAA and PAA, as shown by electro-chromatograms with appropriate standards (Fig 5C). Assuming that those two compounds are the main inducing molecules in the unextracted supernatant of *P. gingivalis*, we evaluated their individual concentration to be in the range of ~4–5 mM based on a dose-response curve with equimolar concentrations of HPAA and PAA (S8E Fig). To validate that a

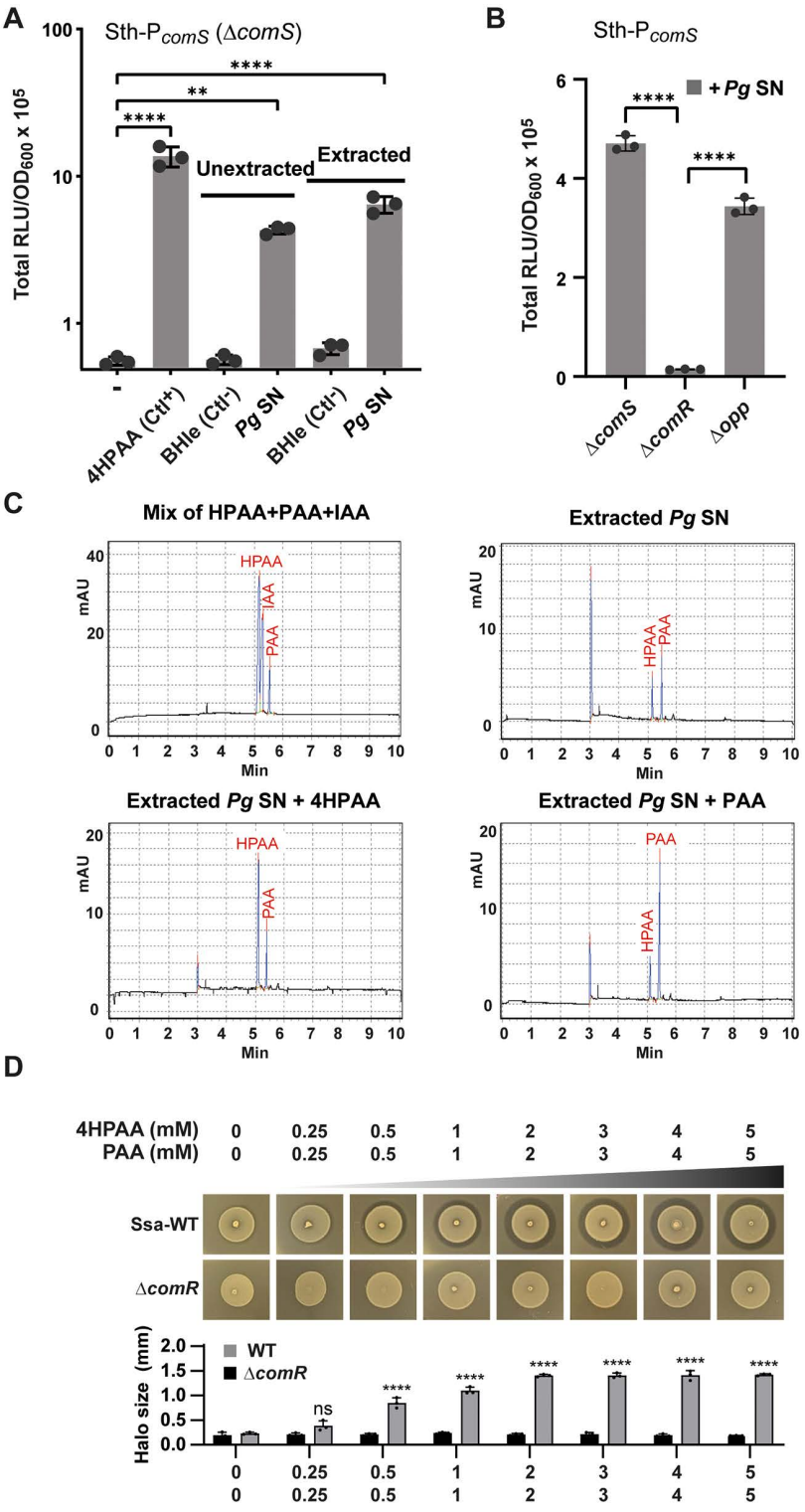

Fig 5. *P. gingivalis* culture supernatant triggers ComR activation. A. Luminescence assays (total RLU/OD_{600}) without addition (−), with 1 mM 4HPAA (positive control), and 25% (vol/vol) of BHIe medium (negative control), filtered *P. gingivalis* supernatant (*Pg* SN), ethyl acetate-extracted BHIe (negative control), and ethyl acetate-extracted *Pg* SN in CDM. Experiments were performed with *S. thermophilus* (Sth) P_{comS}-*luxAB* Δ*comS*. **B.** Luminescence assays (total RLU/OD_{600}) of Δ*comS*, Δ*comR* and Δ*opp* mutants in presence of 25% (vol/vol) of *Pg* SN in CDM. The three mutants are

derivatives of *S. thermophilus* P_{comS}-*luxAB*. **C.** Separation by capillary electrophoresis of ethyl acetate-extracted *P. gingivalis* supernatant. Electrochromatograms display a mixture of 4HPAA (3 mM), IAA (2 mM), and PAA (1 mM) used as standards (top left); extracted *Pg* SN (top right); addition of 0.5 mM 4HPAA to extracted *Pg* SN (bottom left); and addition of 0.5 mM PAA to extracted *Pg* SN (bottom right). **D.** Bacteriocin assays with increasing concentrations of 4HPAA and PAA (each from 0 to 5 mM) on *S. salivarius* (Ssa) wild type (WT) and Δ*comR* mutant (negative control). *Lactococcus lactis* IL1403 was used as an indicator strain. The bottom graph shows the size of inhibition zones (mm). In panels A, B, and D, dots, bars, and error bars show biological (panels A and B) or technical (panel D) triplicates, mean values, and standard deviations, respectively. In panel A, all tested conditions were statistically compared to the control condition without external addition (minus sign). In panel B, the Δ*comS* and Δ*opp* mutants were statistically compared to the Δ*comR* mutant. In panel D, all tested conditions with the WT were statistically compared to the control condition without external addition of 4HPAA and PAA. Statistical analyses used a one-way ANOVA with Dunnett's test (** $P < 0.01$; **** $P < 0.0001$; ns, non-significant). The data underlying this Figure can be found in S1 Data.

https://doi.org/10.1371/journal.pbio.3003718.g005

1:1 mixture of HPAA and PAA can induce bacteriocin production in *S. salivarius* wild type, bacteriocin assays were performed with increasing concentrations of both compounds. Remarkably, growth inhibition was detected at a ~10-fold lower concentration than found in the *P. gingivalis* filtered supernatant (Fig 5D).

Together, these results show that the well-known amino acid degrader, *P. gingivalis* [47,48], secretes enough aromatic amino acid derivatives in the extracellular growth medium to activate predation in salivarius streptococci.

Discussion

Cell-to-cell communication in *Bacillota* (low-GC Gram-positive bacteria) is largely controlled by the RRNPPA superfamily of cytoplasmic QS receptors (~5,000 members identified so far) [22]. Those sensors are involved in a range of key physiological processes such as horizontal gene transfer, metabolism, virulence, sporulation, predation, biofilm formation, and phage lysogeny [22,24]. So far, all the characterized regulators of this superfamily were reported to be activated by small unmodified peptides used as communication pheromones [24]. Notably, we report here that a member of the RRNPPA superfamily could alternate activation by binding its cognate signaling peptide or a specific class of small organic molecules.

In streptococci, the ComR family of RRNPPA is of key importance as signaling regulators for the control of competence and predation [21,22,31]. *S. salivarius* HSISS4 is equipped with three members of this family that coordinate the coupling (via ComR) or the uncoupling (via ScuR/SarF) of predation with competence for DNA transformation [7,8]. In this work, we show an unexpected uncoupling mechanism of predation via ComR by the sensing of byproducts from hydrophobic amino-acid catabolism (named hereafter HACs for hydrophobic amino-acids catabolites) produced by many proteolytic bacteria proliferating in the digestive tract [30] (Fig 6). This parallel layer of predation control by small organic molecules has substantial advantages compared to the classical regulatory cascade of the ComR-XIP system. In its QS mode for intra-species communication, ComRS is quickly shut down by the intracellular degradation of the XIP pheromone (ComX-PepF relay) to avoid an over-activation of competence that could be deleterious for the cell [11]. This mode of control results in a pulse production of bacteriocins (Figs 2A and 6A), which are expected to release extracellular DNA from neighboring bacteria for DNA transformation (fratricide and sobrinicide processes) [6]. In its HAC-responding mode, the ComRS system is not shut down and continuously expresses bacteriocin during growth until the late stages of the exponential phase (Figs 2A and 6B). This continuous production at high cell density would have the huge benefit of accumulating high concentrations of antimicrobial peptides in the ecological niche of *S. salivarius*. Another advantage of responding to small organic molecules is their higher stability compared to signaling peptides, which could be prone to degradation/sequestration in the extracellular medium by a range of QS quenching mechanisms. Interestingly, HACs largely accumulate in human fluids in cases of microbial dysbiosis in the digestive tract, suggesting quite high stability [28–30,43,44]. To conclude, those two modes of ComRS activation not only increase the range of activating stimuli but also improve the capacity of predation in time (no shut-down) and space (unlinked to pheromone availability), an asset for a dominant species in various parts of the digestive tract.

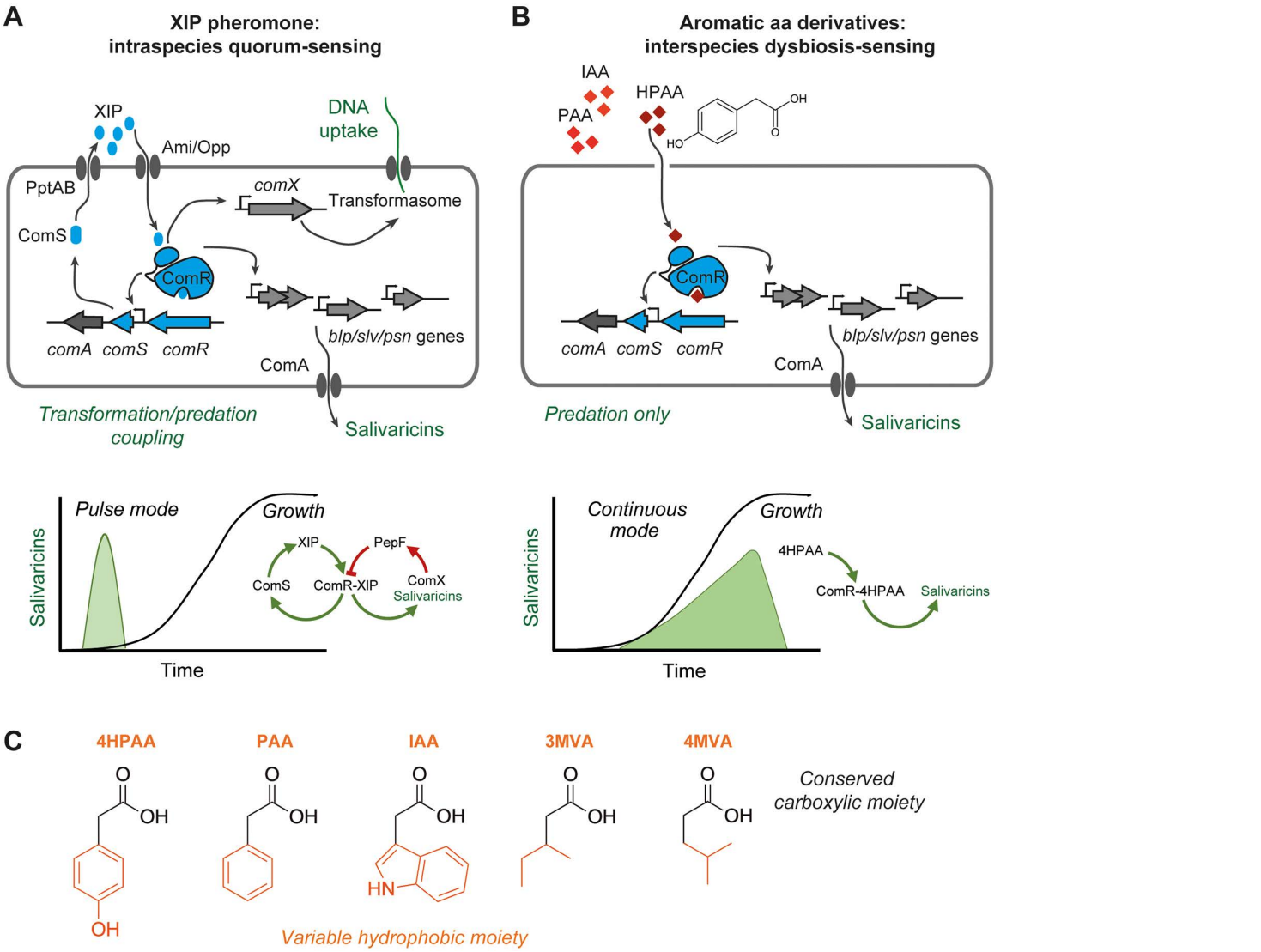

Fig 6. Dual activation of the cytoplasmic sensor ComR by XIP pheromone or aromatic amino acid catabolites in salivarius streptococci. A. Classical activation of the ComRS system by XIP for intraspecies QS, leading to a coactivation of competence (DNA uptake) and predation (salivaricin production). Production of salivaricins takes place in a pulse mode due to a combined positive and negative feedback loop through ComS and the ComX-PepF relay (XIP degradation), respectively. **B.** Pheromone-independent activation of ComR by aromatic amino acid catabolites for interspecies dysbiosis-sensing, leading only to the activation of predation. Production of salivaricins takes place in a continuous mode due to an absence of a negative feedback loop. **C.** Summary of ComR-inducing carboxylic acids comprising a conserved carboxylate moiety and a hydrophobic group, which are derivatives of bulky hydrophobic amino acids.

https://doi.org/10.1371/journal.pbio.3003718.g006

Previously, we showed that $ComR_{Sth}$ activation by XIP required key interactions at both the bottom (XIP-L8 with ComR-T92 and K100) and the top (XIP-L1 with ComR-Y174 and F171) of the binding pocket (Fig 3B) [17,25]. Therefore, the ComR apo-form is double-locked and needs interactions at both sub-sites to be activated by XIP [25]. Based on *in silico* docking, the use of ComR mutants, and a range of HAC analogs, we propose that HACs activate ComR through a lower stabilization of the active holo-form by binding to the bottom sub-site only. The deep part of the XIP-binding pocket in the apo-form is occupied by a network of six interacting water molecules (two are in direct interaction with T90 and

D167) (S9A Fig). As classically proposed for hydrophobic ligands, HAC binding will release those trapped water molecules [49] while being stabilized through ionic and H-bond interactions with key ComR residues (mainly K100, T90, and D167) of the bottom sub-site (Fig 3B). We showed that the size of the binding pocket combined with these specific interactions restricts the range of ligands to a couple of activating molecules (*i.e.*, 4HPAA, 3HPAA, PAA, IAA, 3MVA, and 4MVA), all sharing a carboxylic group associated with a hydrophobic moiety of the appropriate bulkiness (Fig 6C). This model of activation by HACs is strongly supported by the $ComR_{Sth}$ Y174A-F171A variant with a mutated top sub-site, which is insensitive to XIP but strongly activated by the best inducer, 4HPAA. Despite conservation of all key 4HPAA-interacting residues, the absence of activation of ComR from *S. vestibularis*, as well as of the $ComR_{Sth}$-R92G variant, can likely be explained by structural differences in the ligand-binding pocket. Structural modeling indicates that substitution of R92 by glycine in $ComR_{Sth}$—mirroring the native glycine present at the equivalent position in $ComR_{Sve}$ and $ComR_{Smu}$—results in an enlarged binding cavity (S9B Fig). This expansion may increase the number of water molecules occupying both the apo and 4HPAA-bound pockets and alter their relative free energy states, thereby reducing the thermodynamic favorability of 4HPAA binding. Moreover, the intermediate level of $ComR_{Sth}$ activation by HACs compared to XIP likely explains why HACs fail to activate competence through transcriptional induction of *comX* (S2F Fig). Indeed, we previously showed that *comX* transcription is less responsive to ComR activation than bacteriocin genes, due to the presence of a non-canonical ComR-binding box [8]. In this context, although the ComR·HAC complex is predicted—based on docking analyses and functional assays—to be less stabilized than the ComR·XIP complex, this level of stabilization may still be sufficient to promote higher-order complex formation at the *slvX* promoter, but not at the *comX* promoter. Altogether, these two layers of control acting on a single sensor provide a mechanistic basis for the uncoupling between predation activation and competence development.

Aromatic HACs have previously been reported as signaling molecules in different bacterial processes such as plant-bacteria symbiosis [50], virulence shutdown [51], and phase variation control for virulence activation [52]. Among these processes, the molecular mechanism of signaling regulation by HCAs has only been elucidated for invasion through phase variation in *Neisseria meningitidis*, a colonizer of the nasopharynx [52] that is also occupied by *S. salivarius* [53]. In this case, the process is under the control of the stand-alone transcriptional repressor NadR (MarR family), which is directly activated by 4HPAA binding [52,54]. Here, we propose that HACs could act as signaling molecules of dysbiosis resulting from the proliferation of proteolytic bacteria capable of partial degradation of aromatic amino acids. The production of aromatic HACs by bacteria proliferating in the digestive tract has previously been reported for a range of anaerobic gram-negative and -positive bacteria such as the pathobionts *P. gingivalis* [47] and *Clostridioides difficile* [37,55], respectively. In addition, a co-occurrence between their proliferation in the case of dysbiosis and the detection of aromatic HACs in human fluids has been largely documented [28–30,43,44]. As an example, up to 0.1 mM of 4HPAA has been detected in the saliva of patients suffering from periodontal disease [44], a concentration that could be much higher at the site of production. In laboratory conditions, we showed that the periodontal pathogen *P. gingivalis* can produce a mixture of 4HPAA and PAA (mM range) that largely exceeds the minimal concentration required to activate predation in *S. salivarius* (Fig 6). Although the cocktail of bacteriocins produced by the *S. salivarius* strain used in this study did not affect *P. gingivalis* growth in laboratory conditions, it could inhibit *Streptococcus gordonii*, a key mutualist partner of *P. gingivalis* in multi-species communities (S8F Fig) [56]. Interestingly, a recent study showed that lytic bacteriophages targeting *S. gordonii* in model biofilms with *P. gingivalis* were indirectly capable of inhibiting *P. gingivalis* proliferation [57]. So, activation of *S. salivarius* predation by HACs could reshape bacterial communities towards homeostasis through direct or indirect effects on pathobionts.

In conclusion, this study describes an unexpected mode of activation of *S. salivarius* ComR, known as a signaling-peptide cytoplasmic sensor, by a specific class of small organic molecules derived from the anaerobic catabolism of bulky hydrophobic amino acids. This signaling mode may increase the sensory capacity of this beneficial commensal to initiate predation in response to dysbiosis in the human digestive tract. Because many RRNPPA members are pheromone orphans, this research opens a new avenue in chemical communication for the discovery of novel inducing molecules for

Bacillota cytoplasmic sensors. Our results also pave the way for innovative therapeutic strategies where small hydrophobic acids could stimulate bacteriocin production in commensal bacteria to regulate/inhibit pathogen populations.

Materials and methods

Carbon/nitrogen sources, organic acids, and synthetic peptides

Carbon/nitrogen sources from Biolog plates PM1 and PM2A are listed in S1 Table. Organic acids and their suppliers are listed in S2 Table. All organic acids were diluted in water to 100 mM and neutralized with an equimolar amount of NaOH. Synthetic octapeptides XIP_{Sth} (LPYFAGCL) and sBI7 (LPFWLILG) (purity of 95%) and salivaricins BlpK, SlvV, SlvW, SlvX, SlvY, SlvZ, and PsnL [6] were supplied by Peptide 2.0 (Chantilly, VA, USA) and resuspended in 100% dimethyl sulfoxide (DMSO). Final concentration was quantified using a Nanodrop apparatus (ThermoFisher Scientific).

Bacterial strains, plasmids, and oligonucleotides

Bacterial strains, plasmids, and oligonucleotides used in this study are listed and described in the Supporting information (S3 and S4 Tables).

Growth conditions

Escherichia coli TOP10 (Invitrogen) were cultivated with shaking at 37°C in LB (Lysogeny Broth). *S. salivarius* HSISS4 and *S. thermophilus* LMD-9 derivatives were grown at 37°C without shaking in M17 (Difco Laboratories, Detroit, MI) or in CDM [58] supplemented with 1% (w/v) glucose (M17G, CDMG, respectively), except when specified. The Sodium β-glycerophosphate (19 g/l) buffer used in M17 was also added to CDM to increase growth and luminescence induction. *Lactococcus lactis* IL1403 was grown in M17G at 30°C without shaking. *S. gordonii* LMG17843 was grown in liquid M17G or M17G agar plates supplemented with 5% (v/v) defibrinated horse blood (bioMérieux, France) at 37°C. Agar 1.5% (w/v) was added into M17 and LB plates. Solid plates inoculated with *S. salivarius* cells were incubated anaerobically in jars (Oxoid AnaeroGen 2.5 L, Thermo Fischer Scientific) at 37°C. Ampicillin (250 μg ml^{-1}), spectinomycin (200 μg ml^{-1}), chloramphenicol (5 μg ml^{-1}), or erythromycin (10 μg ml^{-1}) were added as required. *P. gingivalis* W83 (ATCC308) cultures were restarted from frozen samples on Columbia agar plates supplemented with yeast extract (5 g l^{-1}), defibrinated horse blood (5% v/v), hemin (25 mg l^{-1}), and menadione (10 mg l^{-1}) at 37°C under a 5% CO_2 atmosphere for 2–3 days. Afterwards, colonies were transferred into liquid Brain Heart Infusion medium supplemented with yeast extract (5 g l^{-1}), hemin (25 mg l^{-1}), and menadione (10 mg l^{-1}) (BHI_e) and incubated for 3–5 days. When needed, 15 mM tyrosine or 15 mM phenylalanine was added to BHIe to stimulate the catabolism of aromatic amino acids. Culture supernatants of cells grown until an OD_{600} of ~1.9 were collected by centrifugation (5,000 *g* for 15 min) and then filtered (0.22 μm). This supernatant was kept at −80°C before its addition to reporter strain cultures.

Construction of mutants and reporter strains

Null mutants were constructed by exchanging (double homologous recombination) the coding sequences (CDS) of target genes (sequence between start and stop codons) for an erythromycin resistance cassette using natural transformation as reported before [8]. Integration of the antibiotic resistance cassette at the right location was subsequently checked by PCR. The promoters of regulator genes (*i.e.*, *comR*, *scuR*, and *sarF*) were fused to the *luxAB* reporter genes and inserted with a chloramphenicol resistance cassette at the permissive tRNA threonine locus (*HSISS4_r00061*) by double homologous recombination. All DNA fragments (S5 Table) were amplified by PCR using the Phusion high-fidelity polymerase (Thermo Fischer Scientific) following a protocol as recommended by the manufacturer. Overlapping PCR products were transferred in competence-induced HSISS4 derivatives, *erm* and *luxAB-cat* cassettes were amplified from pGIUD0855*ery* and pJIM*cat*, respectively.

Luciferase assays

Overnight precultures were diluted at a final OD_{600} of 0.05. Culture samples (300 µl) were incubated in the wells of a sterile covered black microplate with a transparent bottom (Greiner Bio-One, Alphen a/d Rijn, the Netherlands). Growth (OD_{600}) and luciferase (Lux) activity (expressed in relative light units, RLU) were monitored at 10-min intervals during 24 h in a Hidex Sense multimode reader (Hidex, Turku, Finland). Total or maximum specific Lux activity was obtained by dividing Lux activity by the OD_{600} for each measurement and summing all the data obtained over time or selecting the maximum value, respectively. Experimental values represent the averages of at least three independent biological replicates. Statistical analyses of multiple comparisons to the control mean were performed with one-way ANOVA with Dunnett's test. Standard deviations and *P* values were calculated.

For the screening of carbon/nitrogen sources using Phenotype Microarrays (Biolog plates PM1 and PM2A), commercial plates were unsuitable for luminescence assays. The carbon/nitrogen sources from the original plates were initially dissolved in 100 µl of CDM without glucose and incubated for 10 min at 37°C with agitation to ensure complete dissolution. Subsequently, this solution was transferred to the wells of a sterile black microplate with a transparent bottom. A preculture of the reporter strain was added to obtain a final OD_{600} of ~0.05. Glucose from a 25% (w/v) stock solution was added to achieve a final concentration of 0.15% (v/v), and the total volume in each well was adjusted to 300 µl with additional CDM. Growth and luminescence were then monitored as reported above.

Bacteriocin assays

The spot-on-lawn (multilayer) detection method [7] used to test bacteriocin production by *S. salivarius* was performed as follows. Overnight cultures of producer strains were diluted in fresh M17G medium and grown until mid-log phase (OD_{600} of ~0.5). In parallel, we casted plates with a bottom feeding layer (M17G, 1.5% agar) supplemented with inducing molecules (XIP_{Sth}, sBI7, 4HPAA, or 4HPAA + PAA in equimolar ratio), when required. Next, an overnight culture of *L. lactis* IL1403, used as an indicator strain, was incorporated in pre-warmed soft M17G medium (0.3% agar) at a final OD_{600} of 0.05 and casted as a top layer. Finally, we spotted 3 µl of the producer strains on the top layer. Plates were incubated overnight in anaerobic conditions before analysis of the inhibition zones surrounding the producer colonies. Inhibition zones (mm) were measured with the ImageJ software. The size of the inhibition zones was calculated by subtracting the radius of the bacterial spot from the radius of the inhibition halo.

A variation of the above procedure was applied to test the activity of chemically-synthesized salivaricins against *P. gingivalis* W83 and *S. gordonii* LMG17843. Stationary-phase cultures (2–3 days) of *P. gingivalis* W83 or diluted overnight cultures (OD_{600} of 0.05) of *S. gordonii* LMG17843 were spread evenly with sterile cotton swabs on their respective solid media using the lawn method. Onto these lawns, 2 µl of synthetic bacteriocin (100 µM) was spotted. Plates were incubated overnight under appropriate growth conditions until lawns were established, after which inhibition zones at the application sites were assessed.

Natural DNA transformation assays

S. salivarius overnight precultures in CDMG were diluted in the same medium at a final OD_{600} of 0.05. After an incubation of 75 min at 37°C, 4HPAA (10 mM) or XIP_{Sth} (5, 200, or 500 nM) and PCR-amplified DNA fragments containing an *erm* gene (Δ*scuR*::*erm*) surrounded by 1.5-kb recombination arms (1 µg) were added. Cells were grown for 4 h at 37°C before plating on selective M17G agar and incubation in anaerobic conditions.

ComR purification

E. coli TOP10 strains containing plasmids pBAD*comR*$_{Sth}$-*streptag* [59] and pBAD*comR*$_{Sve}$-*streptag* [16] were used for the purification of $ComR_{Sth}$-StreptagII and $ComR_{Sve}$-StreptagII proteins, respectively. Protein purification and storage were

performed as previously described [16]. Protein purity was analyzed by SDS-PAGE and protein concentration was measured using a Nanodrop apparatus (Thermo Fisher Scientific).

Electrophoretic mobility shift assays

EMSA assays were performed as previously described [7,16]. Twofold serial dilutions of purified ComR protein (initial concentration of 4 μM) were mixed with a 40-bp dsDNA fragment (40 ng) carrying the ComR box of P_{comS} coupled to the Cy3 fluorophore in the binding buffer. In parallel, a fixed concentration of purified ComR protein (2 μM) was mixed with a gradient dilution of XIP_{Sth} (5, 50, 200, and 1,000 nM) together with $^{Cy3}P_{comS}$ (40 ng). Negative controls were performed in the absence of protein. Samples were incubated at 37°C for 10 min prior to separation on a native 4% to 20% gradient gel (iD PAGE gel; Eurogentec). Carboxylic acids were added to the running buffer (MOPS) at a final concentration of 10 mM. DNA complexes were detected by fluorescence on the Amersham Typhoon biomolecular imager (Cytiva) with bandpass excitation and emission filters of 595/25 nm (Cy3). The double-stranded DNA fragment was obtained from annealing of single-stranded Cy3-labeled (at the 5′ end) and unlabeled oligonucleotides.

Supernatant extraction and analysis by capillary electrophoresis

Considering the water solubility of 4HPAA at different pHs and its solubility in ethyl acetate [46], a dedicated extraction protocol was developed to extract 4HPAA and closely related molecules from *P. gingivalis* culture supernatants. Initially, 4 ml of culture supernatant was acidified using 0.1 ml of concentrated hydrochloric acid (HCl, 37% w/w). Subsequently, 2 ml of ethyl acetate was incorporated into the solution, followed by thorough mixing and a 10-min decantation period. The organic phase was then separated and mixed with a sodium hydroxide (NaOH) solution (2 ml, 0.01 M). After a further 10-min period of decantation, the aqueous phase was isolated, neutralized with HCl (37% w/w), and filtered (0.22 μm).

For analytical characterization, the extracted sample was separated using a capillary electrophoresis apparatus (Capel 105M, Lumex Instruments), with boric acid (0.1 M, pH ~8.5) as the background electrolyte. A bare fused silica capillary of 54/46 cm in total/effective length with an internal diameter of 50 μm from Agilent was used. Samples were injected at a pressure of 30 mbar for 5 s. A voltage of 25 kV was applied throughout the analysis. UV absorbance at 210 nm was used for detection. The capillary temperature was maintained at 20°C during all steps. The analyses were conducted on the sample alone and in the presence of either 0.5 mM 4HPAA or 0.5 mM PAA, allowing for the assessment of the extraction efficiency and the selectivity of the protocol towards 4HPAA and closely related molecules.

4HPAA docking and structure prediction or visualization

For *in silico* docking predictions of 4HPAA in ComR, the EADock DSS engine from SwissDock was used with default parameters [38]. Docking was performed with the crystal structure of 4HPAA (CCDC 274674) in its anionic form. The holoforms of $ComR_{Sth}$ (PDB: 5JUB, chain A) and $ComR_{Sve}$ (PDB: 6HUA, chain A), and the apoform of $ComR_{Sth}$ (PDB: 5JUF, without SO_4 and H_2O molecules) were used as targets. Ab initio modeling of ComR·4HPAA complexes were performed with the protein-ligand prediction tool Chai-1 using default parameters (https://lab.chaidiscovery.com) [40] using 4HPAA in SMILES format and the primary amino-acid sequences of ComR from *S. thermophilus* LMD-9 (GenBank: ABJ65625.1), *S. salivarius* HSISS4 (GenBank: ALR79229.1), *S. vestibularis* F0396 (GenBank: EFQ60116.1), *Streptococcus mutans* UA159 (GenBank: AAN57849.1), *Streptococcus pyogenes* M1 (GenBank: XXA72633.1), and *Streptococcus suis* P1/7 (GenBank: CAR44181.1). Structure predictions of ComR mutants with AlphaFold 2 were obtained from the AlphaFold CoLab notebook using default parameters [60]. The figures with structural elements were prepared by using the graphic software PyMol (http://www.pymol.org/). The multiple amino-acid sequence alignment was performed with the PRALINE program using default parameters (https://www.ibi.vu.nl/programs/) [61].

Supporting information

S1 Fig. Screening of carbon/nitrogen sources using Phenotype Microarrays. Data were obtained with Biolog plates PM1 (**A**) and PM2A (**B**). P_{comR}, P_{scuR}, P_{sarF}, P_{sptA}, P_{slvX}, and P_{comX} reporter fusions (*luxAB*) were tested for maximum light emission (RLU/OD_{600}) in CDM supplemented with 0.15% glucose. Both 4-hydroxyphenylacetic acid (4HPAA) and 3-hydroxyphenylacetic acid (3HPAA) increased luminescence of P_{slvX}, but none of the other promoters. Carbon/nitrogen sources are listed in S1 Table. The data underlying this Figure can be found in S1 Data.
(TIF)

S2 Fig. Impact of XIP and/or 4HPAA on predation and competence in *S. salivarius*. A. Luminescence (RLU/OD_{600}) over time of the *S. salivarius* (Ssa) P_{slvX}-*luxAB* reporter fusion without inducer, with 4HPAA (1 mM), XIP (5 nM), or 4HPAA (1 mM) + XIP (5 nM). **B.** Total luminescence (RLU/OD_{600}) in response to a 4HPAA gradient (0–30 mM) in absence (No XIP) or addition of XIP (5 nM) for *S. salivarius* P_{slvX}-*luxAB*. **C.** Luminescence over time of P_{slvX} activation without inducer, with 4HPAA (1 mM), XIP (25 nM), or 4HPAA (1 mM) + XIP (25 nM). **D.** Luminescence over time of P_{slvX} activation without inducer, with 4HPAA (7.5 mM), XIP (25 nM), or 4HPAA (7.5 mM) + XIP (25 nM). **E.** *S. salivarius* HSISS4 (WT) transformation assays with 4HPAA (10 mM) or XIP (5, 200, and 500 nM), reported to 1 μg of donor DNA per ml. **F.** Fold increase in total luminescence between 4HPAA (10 mM) or XIP (5, 200, and 500 nM) and non-induced conditions for *S. salivarius* P_{slvX} or P_{comX} reporter strain. Data are mean values of biological triplicates ± standard deviation (light color zones in panels A-D). The data underlying this Figure can be found in S1 Data.
(TIF)

S3 Fig. Mobility shift assays to assess direct binding of different organic acids. Mobility shift assays of the *comS* promoter probe (40 ng) conducted with gradients of purified $ComR_{Sth}$ (left) and $ComR_{Sve}$ (right) (Gray triangles, 2:2 dilutions from 4 μM) with 10 mM 4HPAA or 4-methylvaleric acid in the running buffer. Black arrows with a P label are the positions of the probes consisting of Cy3-conjugated DNA fragments of 40 bp. Black arrows with a C label are the position of specific complexes and stars label complexes formed with $ComR_{Sth}$ in presence of organic acids that are not formed with $ComR_{Sve}$ (negative control). The control condition without ComR is indicated with a minus sign (−). For each organic acid, the two parts correspond to samples that were run on the same gel.
(TIF)

S4 Fig. Ab initio modeling of ComR·4HPAA complexes. Representative ComRs are from *S. salivarius* HSISS4 ($ComR_{Ssa}$, GenBank: ALR79229.1), *S. thermophilus* LMD-9 ($ComR_{Sth}$, GenBank: ABJ65625.1), *S. vestibularis* F0396 ($ComR_{Sve}$, GenBank: EFQ60116.1), *Streptococcus mutans* UA159 ($ComR_{Smu}$, GenBank: AAN57849.1), *Streptococcus pyogenes* M1 ($ComR_{Spy}$, GenBank: XXA72633.1), and *Streptococcus suis* P1/7 ($ComR_{Ssu}$, GenBank: CAR44181.1). Candidate residues for interaction with 4HPAA (light blue) in $ComR_{Sth}$ (T90, K100, D167, and N208) or at the same positions in other ComR predicted structures are higlighted in magenta. Residues labeled in red are not conserved. Modeling was performed with the protein-ligand prediction tool Chai-1.
(TIF)

S5 Fig. Multiple alignment of ComR regions containing residues predicted to interact with 4HPAA. Selected ComR regions (amino-acid positions in parentheses, bottom right) are from *S. salivarius* HSISS4 (ComR_Ssa_HSISS4), *S. thermophilus* LMD-9 (ComR_Sth_LMD-9), *S. vestibularis* F0396 (ComR_Sve_F0396), *Streptococcus mutans* UA159 (ComR_Smu_UA159), *Streptococcus pyogenes* M1 (ComR_Spy_M1), and *Streptococcus suis* P1/7 (ComR_Ssu_P1_7). Candidate residues for interaction with 4HPAA in $ComR_{Sth}$ (T90, K100, D167, and N208) are boxed. The multiple sequence alignment was performed with the PRALINE program. The color code for the conservation score (scale 1–10) is indicated on the top.
(TIF)

S6 Fig. In vivo testing of all available $ComR_{Sth}$ mutants involved in XIP_{Sth} binding or selectivity change towards XIP_{Sve}. A. Positioning of the mutated $ComR_{Sth}$ residues in the XIP_{Sth} binding pocket. Mutated residues strongly or partially affecting 4HPAA induction are labeled in red and pink, respectively. Mutated residues showing enhanced 4HPAA activation are labeled in green. Mutated residues, which are neutral regarding 4HPAA induction, are labeled in white. XIP_{Sth} and predicted 4HPAA docking are shown in white and burgundy red, respectively. **B.** In vivo luminescence response (total RLU/OD_{600}) of $ComR_{Sth}$ wild-type (WT) and variants K100A, T90A, Y174A, F171A, and Y174A/F171A to 4HPAA (10 mM) or XIP (5 nM). Experiments were performed with *S. thermophilus* P_{comS}-*luxAB* Δ*comS*. **C.** In vivo luminescence response of $ComR_{Sth}$ wild-type (WT), $ComR_{Sth}$ penta-mutant (5× $ComR^*_{Sth}$), $comR_{Sve}$ WT, and variants R92G, P94K, R92A/P94K, V205A, V201A/V205A, S248G, I290T to 4HPAA (10 mM) or XIP (5 nM). The genetic background used as in panel B. In panels B and C, dots, bars, and error bars show biological triplicates, mean values, and standard deviations, respectively. All variants were statistically compared to $ComR_{Sth}$ WT using one-way ANOVA with Dunnett's test (* $P < 0.05$; *** $P < 0.001$; **** $P < 0.0001$; ns, non-significant). The data underlying this Figure can be found in S1 Data.
(TIF)

S7 Fig. Luminescence assays with hydrophobic amino acids and their organic acid derivatives. A. Structure of hydrophobic amino acids and their organic acid derivatives. The name of chemicals in bold green indicates inducing molecules. **B.** Luminescence assays (total RLU/OD_{600}) with hydrophobic amino acids and their derivatives (10 mM) shown in panel A. Derivatives of Tyr, Phe, Trp, Ile, and Leu induced a signal. Experiments were performed with *S. thermophilus* P_{comS}-*luxAB* Δ*comS* and *S. salivarius* P_{slvX}-*luxAB*. Dots, bars, and error bars show biological triplicates, mean values, and standard deviations, respectively. All variant molecules were statistically compared to their respective control condition without addition of amino acid or organic acid derivative (minus sign) using one-way ANOVA with Dunnett's test (**** $P < 0.0001$; ns, non-significant). The data underlying this Figure can be found in S1 Data.
(TIF)

S8 Fig. Luminescence assays with culture supernatants of *P. gingivalis* and growth inhibition by salvaricins. A. Luminescence assays (total RLU/OD_{600}) of *S. thermophilus* (Sth) P_{comS}-*luxAB* Δ*comS* with 25% (v/v) of uncultured BHIe medium without and with Phe (15 mM), Tyr (15 mM), or 4HPAA (1 mM) (negative and positive controls), filtered *P. gingivalis* supernatant (*Pg* SN), and *Pg* SN with Phe (15 mM) or Tyr (15 mM) in CDM. **B.** Luminescence assays of *S. salivarius* (Ssa) P_{slvX}-*luxAB* as reported in panel A. **C.** Luminescence assays of *S. salivarius* P_{comR}-*luxAB* without (CDM, Ctl) and with 25% (v/v) M17 or BHIe. **D.** Luminescence assays of *S. salivarius* P_{slvX}-*luxAB* P_{xyl2}-*comR* as reported in panel B. The *comR* expression was induced by adding 0.2% xylose. **E.** Luminescence assays of *S. thermophilus* P_{comS}-*luxAB* Δ*comS* with increasing concentration (mM) of a mixture of 4HPAA and PAA (ratio 1:1). Each compound of the mixture was individually resuspended in BHIe medium at the indicated concentration. Twenty-five% (v/v) of BHIe solutions were incorporated in CDM. The red arrow corresponds to the concentration detected in *Pg* SN. **F.** Bacteriocin assays with synthetic versions of salivaricins from *S. salivarius* HSISS4 either used either as a cocktail of 6 peptides or tested separately. The broad-spectrum salivaricin PsnL (not produced by HSISS4) was also tested. *P. gingivalis* W83 and *S. gordonii* LMG 17,843 were used as indicator strains. DMSO (100%) was used as negative control. In panels A to D, dots, bars, and error bars show biological triplicates, mean values, and standard deviations, respectively. All tested conditions were statistically compared to the control (Ctl) using a one-way ANOVA with Dunnett's test (* $P < 0.05$; ** $P < 0.01$; *** $P < 0.001$; **** $P < 0.0001$; ns, non-significant). The data underlying this Figure can be found in S1 Data.
(TIF)

S9 Fig. Mechanism of $ComR_{Sth}$ activation by 4HPAA. A. Position of water molecules (red spheres) in the bottom of the XIP-binding pocket of $ComR_{Sth}$ apoform (PDB 5JUF) (left) compared to the predicted docking of 4HPAA (blue) in $ComR_{Sth}$ holoform (PDB 5JUB) (right). Four out of six water molecules are interacting with residues T90, D167, and N208 in the apoform (in yellow), which are also predicted to interact with 4HPAA in the holoform (in green). **B.** Comparison of the size

of the 4HPAA-binding pocket (light gray) between holo-$ComR_{Sth}$ (PDB 5JUB), $ComR_{Sth}$-R92G (AlphaFold2 model), holo-$ComR_{Sve}$ (PDB 6HUA), and $ComR_{Smu}$ (AlphaFold2 model). The R92G substitution, which abolished 4HPAA induction in $ComR_{Sth}$, is highlighted in red. Residues T90, K100, D167, and N208 (or their equivalent positions) interacting with 4HPAA are colored in mauve. The position of docked 4HPAA (blue-green) in holo-$ComR_{Sth}$ is reported in the other structures.
(TIF)

S1 Table. List of tested carbon/nitrogen sources from Biolog plates PM1 and PM2A.
(PDF)

S2 Table. List of organic acids and amino acids tested in this study.
(PDF)

S3 Table. List of strains and plasmids.
(PDF)

S4 Table. List of oligonucleotides used in this study.
(PDF)

S5 Table. Overlapping and cloning PCR sub-fragments.
(PDF)

S1 Data. All numerical data and statistical analyses used in this work.
(XLSX)

S1 Raw Images. All raw images used in figures.
(PDF)

Author contributions

Conceptualization: Guillaume Cerckel, Johann Mignolet, Patrice Soumillion, Pascal Hols.

Data curation: Guillaume Cerckel, Denis Dereinne, Pascal Hols.

Formal analysis: Guillaume Cerckel, Johann Mignolet, Patrice Soumillion, Pascal Hols.

Funding acquisition: Pascal Hols.

Investigation: Guillaume Cerckel, Denis Dereinne, Laura Ledesma-García, Vincent Meuric, Benoît Desguin.

Methodology: Guillaume Cerckel, Laura Ledesma-García, Vincent Meuric, Benoît Desguin, Patrice Soumillion.

Project administration: Pascal Hols.

Supervision: Johann Mignolet, Patrice Soumillion, Pascal Hols.

Validation: Johann Mignolet, Pascal Hols.

Writing – original draft: Guillaume Cerckel, Patrice Soumillion, Pascal Hols.

Writing – review & editing: Guillaume Cerckel, Vincent Meuric, Benoît Desguin, Johann Mignolet, Patrice Soumillion, Pascal Hols.

References

1. Delorme C, Abraham A-L, Renault P, Guédon E. Genomics of *Streptococcus salivarius*, a major human commensal. Infect Genet Evol. 2015;33:381–92. https://doi.org/10.1016/j.meegid.2014.10.001 PMID: 25311532
2. Hols P, Ledesma-García L, Gabant P, Mignolet J. Mobilization of microbiota commensals and their bacteriocins for therapeutics. Trends Microbiol. 2019;27(8):690–702. https://doi.org/10.1016/j.tim.2019.03.007 PMID: 30987817

3. Tagg JR, Harold LK, Jain R, Hale JDF. Beneficial modulation of human health in the oral cavity and beyond using bacteriocin-like inhibitory substance-producing streptococcal probiotics. Front Microbiol. 2023;14:1161155. https://doi.org/10.3389/fmicb.2023.1161155 PMID: 37056747
4. Ye D, Liu Y, Li J, Zhou J, Cao J, Wu Y, et al. Competitive dynamics and balance between *Streptococcus mutans* and commensal streptococci in oral microecology. Crit Rev Microbiol. 2025;51(3):532–43. https://doi.org/10.1080/1040841X.2024.2389386 PMID: 39132685
5. Couvigny B, Kulakauskas S, Pons N, Quinquis B, Abraham A-L, Meylheuc T, et al. Identification of new factors modulating adhesion abilities of the pioneer commensal bacterium *Streptococcus salivarius*. Front Microbiol. 2018;9:273. https://doi.org/10.3389/fmicb.2018.00273 PMID: 29515553
6. Damoczi J, Knoops A, Martou M-S, Jaumaux F, Gabant P, Mahillon J, et al. Uncovering the arsenal of class II bacteriocins in salivarius streptococci. Commun Biol. 2024;7(1):1511. https://doi.org/10.1038/s42003-024-07217-y PMID: 39543239
7. Mignolet J, Cerckel G, Damoczi J, Ledesma-Garcia L, Sass A, Coenye T, et al. Subtle selectivity in a pheromone sensor triumvirate desynchronizes competence and predation in a human gut commensal. Elife. 2019;8:e47139. https://doi.org/10.7554/eLife.47139 PMID: 31433299
8. Mignolet J, Fontaine L, Sass A, Nannan C, Mahillon J, Coenye T, et al. Circuitry rewiring directly couples competence to predation in the gut dweller *Streptococcus salivarius*. Cell Rep. 2018;22(7):1627–38. https://doi.org/10.1016/j.celrep.2018.01.055 PMID: 29444418
9. Fontaine L, Wahl A, Fléchard M, Mignolet J, Hols P. Regulation of competence for natural transformation in streptococci. Infect Genet Evol. 2015;33:343–60. https://doi.org/10.1016/j.meegid.2014.09.010 PMID: 25236918
10. Knoops A, Vande Capelle F, Fontaine L, Verhaegen M, Mignolet J, Goffin P, et al. The CovRS environmental sensor directly controls the ComRS signaling system to orchestrate competence bimodality in salivarius streptococci. mBio. 2022;13(1):e0312521. https://doi.org/10.1128/mbio.03125-21 PMID: 35089064
11. Knoops A, Ledesma-García L, Waegemans A, Lamontagne M, Decat B, Degand H, et al. Competence shut-off by intracellular pheromone degradation in salivarius streptococci. PLoS Genet. 2022;18(5):e1010198. https://doi.org/10.1371/journal.pgen.1010198 PMID: 35613247
12. Knoops A, Waegemans A, Lamontagne M, Decat B, Mignolet J, Veening JW. A genome-wide CRISPR interference screen reveals an StkP-mediated connection between cell wall integrity and competence in *Streptococcus salivarius*. mSystems. 2022;7(6):e0073522. https://doi.org/10.1128/msystems.00735-22
13. García-Curiel L, Del Rocío López-Cuellar M, Rodríguez-Hernández AI, Chavarría-Hernández N. Toward understanding the signals of bacteriocin production by *Streptococcus* spp. and their importance in current applications. World J Microbiol Biotechnol. 2021;37(1):15. https://doi.org/10.1007/s11274-020-02973-5 PMID: 33394178
14. Johnsborg O, Eldholm V, Håvarstein LS. Natural genetic transformation: prevalence, mechanisms and function. Res Microbiol. 2007;158(10):767–78. https://doi.org/10.1016/j.resmic.2007.09.004 PMID: 17997281
15. Martin B, Soulet A-L, Mirouze N, Prudhomme M, Mortier-Barrière I, Granadel C, et al. ComE/ComE~P interplay dictates activation or extinction status of pneumococcal X-state (competence). Mol Microbiol. 2013;87(2):394–411. https://doi.org/10.1111/mmi.12104 PMID: 23216914
16. Ledesma-Garcia L, Thuillier J, Guzman-Espinola A, Ensinck I, Li de la Sierra-Gallay I, Lazar N, et al. Molecular dissection of pheromone selectivity in the competence signaling system ComRS of streptococci. Proc Natl Acad Sci U S A. 2020;117(14):7745–54. https://doi.org/10.1073/pnas.1916085117 PMID: 32198205
17. Talagas A, Fontaine L, Ledesma-García L, Mignolet J, Li de la Sierra-Gallay I, Lazar N, et al. Structural insights into streptococcal competence regulation by the cell-to-cell communication system ComRS. PLoS Pathog. 2016;12(12):e1005980. https://doi.org/10.1371/journal.ppat.1005980 PMID: 27907189
18. Gardan R, Besset C, Gitton C, Guillot A, Fontaine L, Hols P, et al. Extracellular life cycle of ComS, the competence-stimulating peptide of *Streptococcus thermophilus*. J Bacteriol. 2013;195(8):1845–55. https://doi.org/10.1128/JB.02196-12 PMID: 23396911
19. Fontaine L, Boutry C, de Frahan MH, Delplace B, Fremaux C, Horvath P, et al. A novel pheromone quorum-sensing system controls the development of natural competence in *Streptococcus thermophilus* and *Streptococcus salivarius*. J Bacteriol. 2010;192(5):1444–54. https://doi.org/10.1128/JB.01251-09 PMID: 20023010
20. Shanker E, Federle MJ. Quorum sensing regulation of competence and bacteriocins in *Streptococcus pneumoniae* and *mutans*. Genes (Basel). 2017;8(1):15. https://doi.org/10.3390/genes8010015 PMID: 28067778
21. Caillot Q, Guillot A, Lacroix T, Oliveira-Correia L, Huillet E, André G, et al. RRNPP quorum-sensing repertoires in the salivarius group genomes: overrepresentation and synchronous activation of SHP/Rgg systems in *Streptococcus thermophilus*. J Bacteriol. 2025;207(9):e0023125. https://doi.org/10.1128/jb.00231-25 PMID: 40856484
22. Felipe-Ruiz A, Marina A, Rocha EPC. Structural and genomic evolution of RRNPPA systems and their pheromone signaling. mBio. 2022;13(6):e0251422. https://doi.org/10.1128/mbio.02514-22 PMID: 36259720
23. Moi D, Bernard C, Steinegger M, Nevers Y, Langleib M, Dessimoz C. Structural phylogenetics unravels the evolutionary diversification of communication systems in gram-positive bacteria and their viruses. Nat Struct Mol Biol. 2025;32(12):2492–502. https://doi.org/10.1038/s41594-025-01649-8 PMID: 41073779
24. Neiditch MB, Capodagli GC, Prehna G, Federle MJ. Genetic and structural analyses of RRNPP intercellular peptide signaling of gram-positive bacteria. Annu Rev Genet. 2017;51:311–33. https://doi.org/10.1146/annurev-genet-120116-023507 PMID: 28876981
25. Ledesma-García L, Ensinck I, Dereinne D, Viela F, Mignolet J, Dufrêne YF, et al. Coevolution of the bacterial pheromone ComS and sensor ComR fine-tunes natural transformation in streptococci. J Biol Chem. 2021;297(6):101346. https://doi.org/10.1016/j.jbc.2021.101346 PMID: 34715127

26. Abranches J, Zeng L, Kajfasz JK, Palmer SR, Chakraborty B, Wen ZT, et al. Biology of oral streptococci. Microbiol Spectr. 2018;6(5). https://doi.org/10.1128/microbiolspec.GPP3-0042-2018
27. Shimizu H, Miyamoto J, Hisa K, Ohue-Kitano R, Takada H, Yamano M, et al. Sucrose-preferring gut microbes prevent host obesity by producing exopolysaccharides. Nat Commun. 2025;16(1):1145. https://doi.org/10.1038/s41467-025-56470-0 PMID: 39880823
28. Lee Y-T, Huang S-Q, Lin C-H, Pao L-H, Chiu C-H. Quantification of gut microbiota dysbiosis-related organic acids in human urine using LC-MS/MS. Molecules. 2022;27(17):5363. https://doi.org/10.3390/molecules27175363 PMID: 36080134
29. Liebsch C, Pitchika V, Pink C, Samietz S, Kastenmüller G, Artati A, et al. The saliva metabolome in association to oral health status. J Dent Res. 2019;98(6):642–51. https://doi.org/10.1177/0022034519842853 PMID: 31026179
30. Russell WR, Duncan SH, Scobbie L, Duncan G, Cantlay L, Calder AG, et al. Major phenylpropanoid-derived metabolites in the human gut can arise from microbial fermentation of protein. Mol Nutr Food Res. 2013;57(3):523–35. https://doi.org/10.1002/mnfr.201200594 PMID: 23349065
31. Fleuchot B, Gitton C, Guillot A, Vidic J, Nicolas P, Besset C, et al. Rgg proteins associated with internalized small hydrophobic peptides: a new quorum-sensing mechanism in streptococci. Mol Microbiol. 2011;80(4):1102–19. https://doi.org/10.1111/j.1365-2958.2011.07633.x PMID: 21435032
32. Aggarwal SD, Yesilkaya H, Dawid S, Hiller NL. The pneumococcal social network. PLoS Pathog. 2020;16(10):e1008931. https://doi.org/10.1371/journal.ppat.1008931 PMID: 33119698
33. Hu D, Laczkovich I, Federle MJ, Morrison DA. Identification and characterization of negative regulators of Rgg1518 quorum sensing in *Streptococcus pneumoniae*. J Bacteriol. 2023;205(7):e0008723. https://doi.org/10.1128/jb.00087-23 PMID: 37341600
34. Kaspar J, Shields RC, Burne RA. Competence inhibition by the XrpA peptide encoded within the comX gene of *Streptococcus mutans*. Mol Microbiol. 2018;109(3):345–64. https://doi.org/10.1111/mmi.13989 PMID: 29802741
35. Rutbeek NR, Rezasoltani H, Patel TR, Khajehpour M, Prehna G. Molecular mechanism of quorum sensing inhibition in *Streptococcus* by the phage protein paratox. J Biol Chem. 2021;297(3):100992. https://doi.org/10.1016/j.jbc.2021.100992 PMID: 34298018
36. Chang JC, Jimenez JC, Federle MJ. Induction of a quorum sensing pathway by environmental signals enhances group A streptococcal resistance to lysozyme. Mol Microbiol. 2015;97(6):1097–113. https://doi.org/10.1111/mmi.13088 PMID: 26062094
37. Barker HA. Amino acid degradation by anaerobic bacteria. Annu Rev Biochem. 1981;50:23–40. https://doi.org/10.1146/annurev.bi.50.070181.000323 PMID: 6791576
38. Grosdidier A, Zoete V, Michielin O. SwissDock, a protein-small molecule docking web service based on EADock DSS. Nucleic Acids Res. 2011;39(Web Server issue):W270-7. https://doi.org/10.1093/nar/gkr366 PMID: 21624888
39. Meyer EA, Castellano RK, Diederich F. Interactions with aromatic rings in chemical and biological recognition. Angew Chem Int Ed Engl. 2003;42(11):1210–50. https://doi.org/10.1002/anie.200390319 PMID: 12645054
40. Discovery C, Boitreaud J, Dent J, McPartlon M, Meier J, Reis V, et al. Chai-1: decoding the molecular interactions of life. bioRxiv. 2024. https://doi.org/10.1101/2024.10.10.615955
41. Cavaco C, Pereira JAM, Taunk K, Taware R, Rapole S, Nagarajaram H, et al. Screening of salivary volatiles for putative breast cancer discrimination: an exploratory study involving geographically distant populations. Anal Bioanal Chem. 2018;410(18):4459–68. https://doi.org/10.1007/s00216-018-1103-x PMID: 29732495
42. De Filippis F, Vannini L, La Storia A, Laghi L, Piombino P, Stellato G, et al. The same microbiota and a potentially discriminant metabolome in the saliva of omnivore, ovo-lacto-vegetarian and Vegan individuals. PLoS One. 2014;9(11):e112373. https://doi.org/10.1371/journal.pone.0112373 PMID: 25372853
43. Pei J, Li F, Xie Y, Liu J, Yu T, Feng X. Microbial and metabolomic analysis of gingival crevicular fluid in general chronic periodontitis patients: lessons for a predictive, preventive, and personalized medical approach. EPMA J. 2020;11(2):197–215. https://doi.org/10.1007/s13167-020-00202-5 PMID: 32547651
44. Takahama U, Imamura H, Hirota S. Nitration of the salivary component 4-hydroxyphenylacetic acid in the human oral cavity: enhancement of nitration under acidic conditions. Eur J Oral Sci. 2009;117(5):555–62. https://doi.org/10.1111/j.1600-0722.2009.00671.x PMID: 19758252
45. Nadaf R, Kumbar VM, Ghagane S. Unravelling the intricacies of *Porphyromonas gingivalis*: virulence factors, lifecycle dynamics and phytochemical interventions for periodontal disease management. APMIS. 2024;132(9):611–24. https://doi.org/10.1111/apm.13440 PMID: 39030947
46. Gracin S, Rasmuson ÅC. Solubility of phenylacetic acid, p-hydroxyphenylacetic acid, p-aminophenylacetic acid, p-hydroxybenzoic acid, and ibuprofen in pure solvents. J Chem Eng Data. 2002;47(6):1379–83. https://doi.org/10.1021/je0255170
47. Bourgeau G, Mayrand D. Phenylacetic acid production by *Bacteroides gingivalis* from phenylalanine and phenylalanine-containing peptides. Can J Microbiol. 1983;29(9):1184–9. https://doi.org/10.1139/m83-181 PMID: 6652581
48. Ding J, Tan L, Wu L, Li J, Zhang Y, Shen Z, et al. Regulation of tryptophan-indole metabolic pathway in *Porphyromonas gingivalis* virulence and microbiota dysbiosis in periodontitis. NPJ Biofilms Microbiomes. 2025;11(1):37. https://doi.org/10.1038/s41522-025-00669-y PMID: 40011497
49. Snyder PW, Mecinovic J, Moustakas DT, Thomas SW 3rd, Harder M, Mack ET, et al. Mechanism of the hydrophobic effect in the biomolecular recognition of arylsulfonamides by carbonic anhydrase. Proc Natl Acad Sci U S A. 2011;108(44):17889–94. https://doi.org/10.1073/pnas.1114107108 PMID: 22011572
50. Spaepen S, Vanderleyden J. Auxin and plant-microbe interactions. Cold Spring Harb Perspect Biol. 2011;3(4):a001438. https://doi.org/10.1101/cshperspect.a001438 PMID: 21084388

51. Ahator SD, Zhang L. Small is mighty-chemical communication systems in *Pseudomonas aeruginosa*. Annu Rev Microbiol. 2019;73:559–78. https://doi.org/10.1146/annurev-micro-020518-120044 PMID: 31226024

52. Metruccio MME, Pigozzi E, Roncarati D, Berlanda Scorza F, Norais N, Hill SA, et al. A novel phase variation mechanism in the meningococcus driven by a ligand-responsive repressor and differential spacing of distal promoter elements. PLoS Pathog. 2009;5(12):e1000710. https://doi.org/10.1371/journal.ppat.1000710 PMID: 20041170

53. Oishi T, Muratani T, Tanaka T, Sato M, Urara K, Ouchi K, et al. Study of normal flora in the pharynx of healthy children. Jpn J Infect Dis. 2021;74(5):450–7. https://doi.org/10.7883/yoken.JJID.2020.824 PMID: 33642434

54. Liguori A, Malito E, Lo Surdo P, Fagnocchi L, Cantini F, Haag AF, et al. Molecular basis of ligand-dependent regulation of NadR, the transcriptional repressor of meningococcal virulence factor NadA. PLoS Pathog. 2016;12(4):e1005557. https://doi.org/10.1371/journal.ppat.1005557 PMID: 27105075

55. Elsden SR, Hilton MG, Waller JM. The end products of the metabolism of aromatic amino acids by Clostridia. Arch Microbiol. 1976;107(3):283–8. https://doi.org/10.1007/BF00425340 PMID: 1275638

56. Kuboniwa M, Houser JR, Hendrickson EL, Wang Q, Alghamdi SA, Sakanaka A, et al. Metabolic crosstalk regulates *Porphyromonas gingivalis* colonization and virulence during oral polymicrobial infection. Nat Microbiol. 2017;2(11):1493–9. https://doi.org/10.1038/s41564-017-0021-6 PMID: 28924191

57. Wu C, Fujiki J, Mathieu J, Schwarz C, Cornell C, Alvarez PJJ. Phage-based biocontrol of *Porphyromonas gingivalis* through indirect targeting. Appl Environ Microbiol. 2024;90(10):e0095124. https://doi.org/10.1128/aem.00951-24 PMID: 39248462

58. Letort C, Juillard V. Development of a minimal chemically-defined medium for the exponential growth of *Streptococcus thermophilus*. J Appl Microbiol. 2001;91(6):1023–9. https://doi.org/10.1046/j.1365-2672.2001.01469.x PMID: 11851809

59. Fontaine L, Goffin P, Dubout H, Delplace B, Baulard A, Lecat-Guillet N, et al. Mechanism of competence activation by the ComRS signalling system in streptococci. Mol Microbiol. 2013;87(6):1113–32. https://doi.org/10.1111/mmi.12157 PMID: 23323845

60. Varadi M, Anyango S, Deshpande M, Nair S, Natassia C, Yordanova G, et al. AlphaFold Protein Structure Database: massively expanding the structural coverage of protein-sequence space with high-accuracy models. Nucleic Acids Res. 2022;50(D1):D439–44. https://doi.org/10.1093/nar/gkab1061 PMID: 34791371

61. Bawono P, Heringa J. PRALINE: a versatile multiple sequence alignment toolkit. Methods Mol Biol. 2014;1079:245–62. https://doi.org/10.1007/978-1-62703-646-7_16 PMID: 24170407